9-22-2022

Sinistral shear during Middle Jurassic emplacement of the Matancilla Plutonic Complex in northern Chile (25.4° S) as evidence of oblique plate convergence during the early Andean orogeny

S. P. Mavor

J. S. Singleton

G. Heuser

R. Gomila

N. M. Seymour

See next page for additional authors

Authors

S. P. Mavor, J. S. Singleton, G. Heuser, R. Gomila, N. M. Seymour, S. Williams, and G. Arancibia

Journal of South American Earth Sciences 120 (2022) 104047

Contents lists available at ScienceDirect

Journal of South American Earth Sciences

journal homepage: www.elsevier.com/locate/jsames

Sinistral shear during Middle Jurassic emplacement of the Matancilla Plutonic Complex in northern Chile (25.4° S) as evidence of oblique plate convergence during the early Andean orogeny

S.P. Mavor [a,b,*], J.S. Singleton [a], G. Heuser [c], R. Gomila [d], N.M. Seymour [e,f], S. Williams [g], G. Arancibia [c]

[a] Department of Geosciences, Colorado State University, Fort Collins, CO, USA
[b] Now at U.S. Geological Survey, Flagstaff, AZ, USA
[c] Departamento de Ingeniería Estructural y Geotécnica, Pontificia Universidad Católica de Chile, Santiago, Chile
[d] Dipartimento di Geoscienze, Università degli Studi di Padova, Padua, Italy
[e] Department of Geological Sciences, Stanford University, Stanford, CA, USA
[f] Department of Earth and Planetary Sciences, University of California Santa Cruz, Santa Cruz, CA, USA
[g] Department of Earth, Environmental and Planetary Sciences, Rice University, Houston, TX, USA

A B S T R A C T

Arc magmatism in a continental subduction zone facilitates rheological weakening of the rigid upper plate, and can accommodate the partitioned trench-parallel component of oblique subduction into an intra-arc shear zone. We document a shear zone at latitude 25.4° S near Taltal, Chile that was associated with intrusion of the Matancilla Plutonic Complex at ~169 Ma to evaluate intra-arc deformation and possible tectonic plate configurations during this time period. Polyphase folding of Paleozoic metasedimentary rocks is overprinted by mylonitic fabrics that are most extensive in a zone up to 1.4 km wide in the thermal aureole of the granodioritic Matancilla pluton, where contact metamorphic andalusite porphyroblasts are synkinematic with fabric development. Mylonite in metasedimentary rocks is overprinted by a ~130 Ma granodiorite (zircon U–Pb) and by ~133 Ma postkinematic monazite (U–Pb). Within the Jurassic Matancilla granodiorite, pervasive ductile shear occurs along the intrusive contact while centimeter-scale discrete high-strain zones throughout the pluton are associated with focused hydrothermal alteration and reaction weakening. Mylonitic foliation in the metasedimentary rocks and within the pluton strikes N- to NE and dips steeply, while stretching lineations are subhorizontal on average. Kinematic indicators record dominantly sinistral shear, though some dextral or symmetric indicators and S > L fabrics suggest a component of coaxial strain and flattening. Sinistral strike-slip kinematics in the Matancilla shear zone may indicate that Middle Jurassic convergence had sinistral obliquity that was locally partitioned into the contemporaneous magmatic arc. Sinistral-oblique convergence would require the Phoenix-Farallon spreading center to be north of ~25° S in the Middle Jurassic, providing a constraint to plate reconstructions during the early Andean orogeny.

1. Introduction

The Andean margin in northern Chile has long stood as a classic example of convergent margin tectonics. Subduction and arc magmatism of the Andean margin has been ongoing since at least the Late Triassic (e.g., del Rey et al., 2016; Coloma et al., 2017; Rodríguez et al., 2019; Jara et al., 2021b) and spans several kinematic shifts in plate margin obliquity. Plate reconstruction models depict a shift from Early Cretaceous sinistral-oblique convergence to the Late Cretaceous dextral-oblique convergence that has persisted to the present. Pre-Cretaceous plate reconstructions have significantly more uncertainty than post-Cretaceous reconstructions given the limited preservation of seafloor isochrons (see Tetley et al., 2019). Recent work continues to explore the older configurations (e.g., Gianni and Navarrete, 2022) but do not incorporate the position of spreading ridges into their discussion. The Farallon-Phoenix spreading center intersected the Gondwana convergent margin in the northern Andes in the Late Triassic, migrated southwards along the margin to central Chile in the Early Jurassic, and returned northwards by the early Late Jurassic (Seton et al., 2012; Matthews et al., 2016; Young et al., 2019, Fig. 1). Subduction convergence vectors at the margin may have changed rapidly as the ridge passed, affecting the kinematics of upper plate deformation. Modeled trench-parallel convergence velocities show a switch from dextral to sinistral obliquity at ~155 Ma at the latitude of Taltal, Chile (25.4° S) shortly after passage of the Farallon-Phoenix spreading center (Maloney et al., 2013; using the kinematic model of Seton et al., 2012),

* Corresponding author. Now at U.S. Geological Survey, Flagstaff, AZ, USA.
E-mail address: smavor@usgs.gov (S.P. Mavor).

https://doi.org/10.1016/j.jsames.2022.104047
Received 27 July 2022; Received in revised form 21 September 2022; Accepted 22 September 2022
Available online 27 September 2022

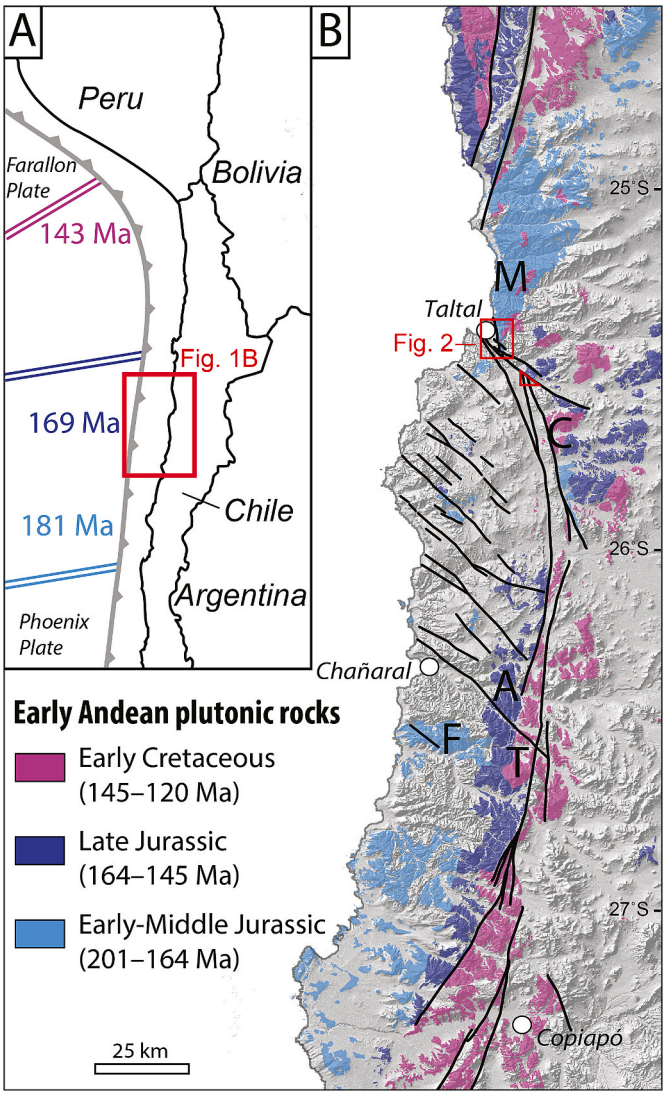

Fig. 1. Paleotectonic setting along the western border of South America. A) Approximate locations of the mid-ocean ridge between the Farallon (north) and Phoenix (south) plates through the Jurassic and Early Cretaceous (from Matthews et al., 2016). B) Shaded relief image with plutonic provinces of the early Andean arc and major Mesozoic fault systems (black lines). Notable plutonic complexes with syn-emplacement ductile shear zones are marked: A – Animas, C – Cerro del Pingo, F – Flamenco, M – Matancilla, T – Las Tazas. Figure modified from Seymour et al. (2020) with data sourced from Álvarez et al. (2016), Arévalo (2005), Contreras et al. (2013), Escribano et al. (2013), Espinoza et al. (2014), Godoy et al. (2003), Godoy and Lara (1998), Godoy and Lara (1999), and Lara and Godoy (1998). Red box indicates the study site (Fig. 2).

but uncertainty in the regional-level details of global Jurassic plate reconstructions and complications from processes such as terrain accretion or discontinuous subduction preclude a firm understanding of when such kinematic switches may have occurred.

A component of syn-convergent Jurassic extension across the Andean arc is suggested by the steady accumulation of marine back-arc basin deposits (Scheuber et al., 1994; Charrier et al., 2007), normal faults that accommodated E-W extension in arc volcaniclastic strata (Dallmeyer et al., 1996), and arc geochemistry with low crustal contribution consistent with extensional tectonics and thinning of the upper plate (Oliveros et al., 2020; Jara et al., 2021b). In the Coastal Cordillera, systematic dike orientations appear to record a transition from E-W extension to NNE-SSW extension and sinistral plate margin obliquity from the Late Jurassic to Early Cretaceous (Taylor and Randall, 2000). However, Late Jurassic dikes with NW-SE dilation could alternatively suggest dextral obliquity or decoupling of onshore deformation from the down-going slab (Scheuber and Gonzalez, 1999).

Other attempts to infer plate margin obliquity leverage syn-magmatic ductile shear zones. Across the Mesozoic Andean margin, phases of ductile deformation have been spatially and temporally restricted to areas adjacent to plutonic bodies where thermal weakening elevated the geothermal gradient above the brittle-plastic transition and enabled mylonitic strain (e.g., Brown et al., 1993; Seymour et al., 2020). One example is recorded along the Early Cretaceous Atacama fault system (AFS; Scheuber and Andriessen, 1990; Seymour et al., 2020), where the margin-parallel component of oblique subduction was partitioned into the arc as sinistral shear and mylonitic fabrics are limited to the thermal aureoles of Cretaceous plutons. Some studies have suggested that Jurassic ductile shear was a necessary precursor to strain localization along the AFS (Scheuber and Andriessen, 1990; Scheuber and Gonzalez, 1999; Rodríguez et al., 2021; Masoch et al., 2021). Ductile shear is not universally associated with Jurassic plutonism; some Jurassic plutons lack any associated penetrative strain (Seymour et al., 2020) while others such as the Late Jurassic Las Animas pluton have syn-magmatic shear zones with down-dip lineations interpreted to reflect progressive stages of pluton emplacement in an E-W extensional environment (Grocott and Taylor, 2002).

The reported absence of strike-slip shear in plutonism-associated deformation envelopes led Dallmeyer et al. (1996) to suggest the plate convergence vector was perpendicular to the margin through the Jurassic and rapidly switched to a sinistral oblique regime recorded by sinistral shear in the mid-Early Cretaceous Las Tazas pluton. This assertion is challenged by more recent work that finds evidence for sinistral ductile shear in the Early Jurassic (Scheuber and Gonzalez, 1999; Rodríguez et al., 2021), even associated with intrusions that were previously considered to record only extensional deformation. Dip-slip extensional (Grocott and Taylor, 2002), sinistral strike-slip (Scheuber and Andriessen, 1990), and sinistral transpressional (Rodríguez et al., 2021) ductile shear zones are recognized for mylonitic Early Jurassic plutons. Observations of strike-slip shear in the magmatic arc and extension in the back arc can be unified by a model of strain partitioning, where the margin-parallel component of oblique subduction is accommodated in a thermally-weakened zone at the arc axis, and the margin-normal component is accommodated inboard of the arc.

These studies show syn-magmatic ductile deformation associated with Jurassic plutonism provides an opportunity to evaluate plate-boundary kinematics of the early Andean orogeny. Partitioning of sinistral-oblique subduction is well established for the Early Cretaceous; however, few constraints have been presented for the Middle Jurassic strain regime. Here we document a sinistral strike-slip shear zone that developed synchronously with the intrusion of the ~169 Ma Matancilla Plutonic Complex. This shear zone (herein referred to as the Matancilla shear zone) provides a new constraint on the Middle Jurassic strain regime of the Andean orogeny and may record partitioning of the margin-parallel component of SE-directed oblique subduction into the contemporaneous magmatic arc.

2. Geologic setting

The pre-Andean history in the Coastal Cordillera of northern Chile is chiefly recorded by late Paleozoic accretionary complexes deposited on the western margin of Gondwana (Díaz-Alvarado et al., 2019). Relatively sparse late Paleozoic and Triassic magmatism gave way to voluminous Jurassic and Early Cretaceous arc magmatism of the Andean orogeny that dominates the geology of the Coastal Cordillera (Fig. 1B). This was accompanied by steady back-arc sedimentation recorded by thick marine stratigraphic packages located ~100 km east of the Coastal Cordillera (Prinz et al., 1994). In the late Early Cretaceous, eastward migration of the magmatic arc and uplift of the former back-arc deposits

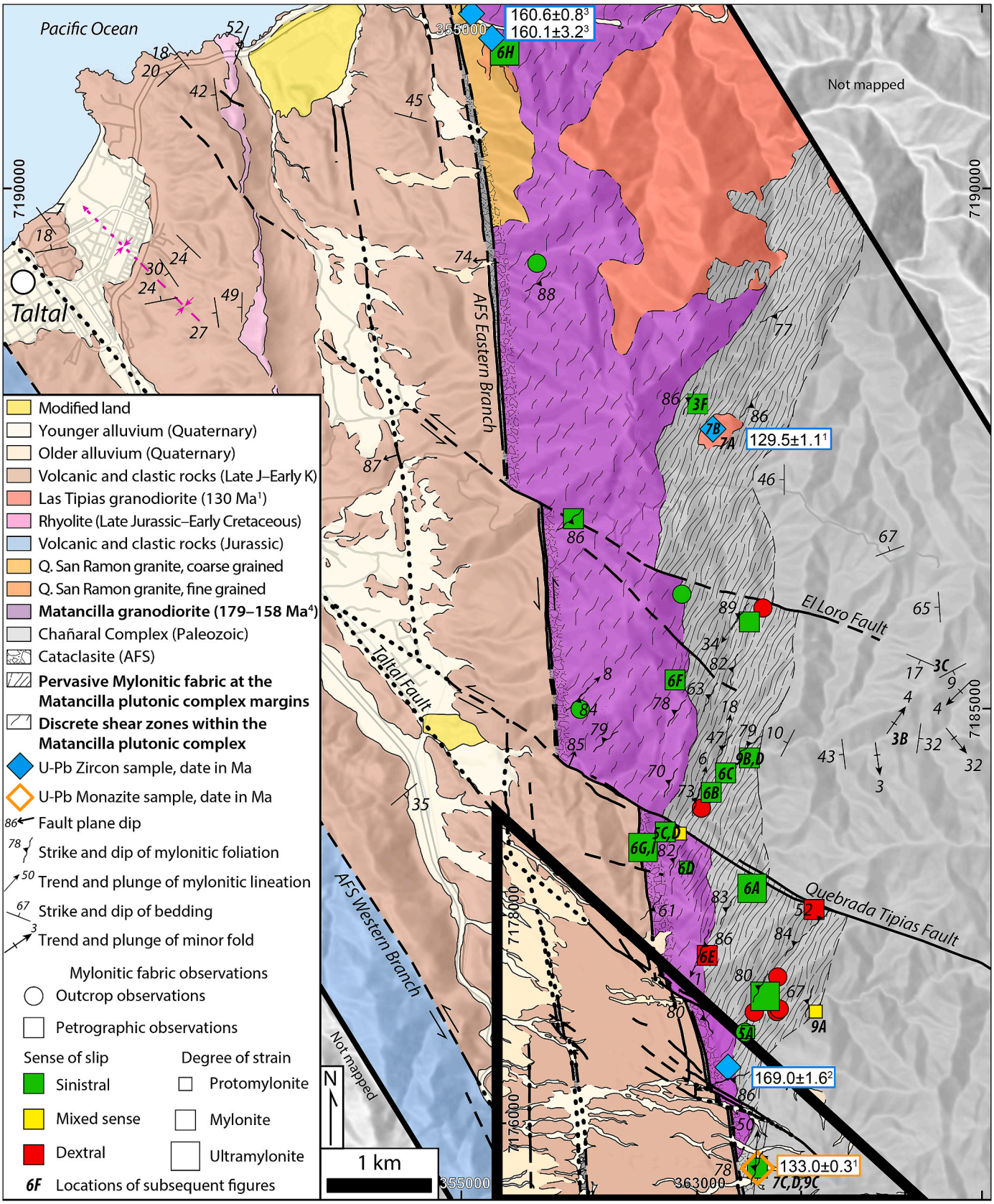

Fig. 2. Geologic map of the Matancilla Plutonic Complex near Taltal, modified from Mavor et al. (2020). An inset map (heavy black outline) with a separate coordinate grid shows the offset sliver of the Matancilla Plutonic Complex south of the Taltal fault in a restored position. Slip on other NW-striking faults of the Cretaceous Taltal fault system has not been restored. U/Pb dates are from: [1]This study; [2]Mavor et al. (2020); [3]Seymour et al. (2021); [4]Escribano et al. (2013). Coordinate system: WGS 1984 19S.

mark a major shift in the dynamics of the Andean orogeny (Charrier et al., 2007).

In the Coastal Cordillera near Taltal (Fig. 1), upper crustal plutons of the arc and volcaniclastic equivalents intrude and overlap Paleozoic metaturbidites of the Chañaral Epimetamorphic Complex of Godoy and Lara (1998), with the oldest Permian plutons crosscutting lower greenschist-facies metamorphic fabrics of the Chañaral Mélange (Bell, 1982). Polyphase SW-vergent folding of tectonic mélange in the Chañaral Epimetamorphic Complex near the city of Chañaral likely records underthrusting of an accretionary prism during late Paleozoic NE-directed oblique subduction on the western margin of Gondwana (Bell, 1984; Fuentes et al., 2016, 2019). Near Taltal, the Chañaral Epimetamorphic Complex is typified by alternating quartzite and phyllite intervals and lacks the basaltic flows, dacitic tuffs, and rhyolites observed further south (Bell, 1984; Fuentes et al., 2018). Reported Paleozoic deformation at this latitude, outside of the mélange zone, is limited to NNE-plunging folds (Escribano et al., 2013).

Triassic igneous rocks with petrographic and geochemical hallmarks of subduction zone magmatism are present in the Coastal Cordillera (Coloma et al., 2017; Rodríguez et al., 2019; Jara et al., 2021b), but the main phase of arc-related Andean magmatism near Taltal began in the Late Jurassic and peaked in the Early Cretaceous (Seymour et al., 2020; Jara et al., 2021a). Mapping near Taltal documents volcanic-dominated and plutonic-dominated domains separated by the AFS, with the deepest structural levels exposed east of the AFS eastern branch (e.g., Escribano et al., 2013; Espinoza et al., 2014). Here, the Chañaral Epimetamorphic Complex was intruded by the Middle Jurassic Matancilla Plutonic Complex (Fig. 2) during a period of relatively low magmatic flux (Seymour et al., 2020; Jara et al., 2021a). First mapped by Arabasz (1971), and subsequently termed the Matancilla intrusive complex by Escribano et al. (2013), we herein use the term 'plutonic complex' rather than 'intrusive complex' in accordance with the international stratigraphic guide (Murphy and Salvador, 2000). The Matancilla Plutonic Complex includes multiple lithologies including granodiorite, diorite, quartz diorite, and monzogranite, with a range of ages from 178 to 154 Ma (Escribano et al., 2013; Álvarez et al., 2016), though detailed mapping and recent zircon U–Pb geochronology indicates some of these sub-units may instead be separate Late Jurassic to Early Cretaceous intrusions (Mavor et al., 2020; Ruthven et al., 2020; Seymour et al., 2021). Within the area of Fig. 2, the plutonic complex is dominated by a ~169 Ma granodiorite (Mavor et al., 2020).

Early Cretaceous ductile shear began at ~139 Ma on the southern Paposo segment of the Atacama fault system (Hervé, 1987; Ruthven et al., 2020). Variably strained plutons show that the northern part of the El Salado segment of the AFS was active between 132 and 119 Ma (Seymour et al., 2020); biotite and hornblende that recrystallized during development of mylonitic fabrics have $^{40}Ar/^{39}Ar$ dates between ~128 and 126 Ma (Espinoza et al., 2014). Brittle AFS deformation continued until 114–110 Ma, when the AFS was cut by the NW-striking Taltal fault system as plutonism ended in the area (Mavor et al., 2020; Seymour et al., 2020). Where the spatial patterns, geometry, and timing of AFS-related mylonitic deformation are well documented along the northern El Salado segment (e.g., near the Cerro del Pingo tonalite; Espinoza et al., 2014; Seymour et al., 2020, 2021), mylonitic fabrics with subhorizontal lineations and sinistral shear sense indicators are oriented parallel with, or slightly clockwise to the vertical N–S fault system. The highest strain fabrics are in screens of Chañaral Epimetamorphic Complex metasedimentary rocks between the AFS and Early Cretaceous plutons. Plutonic rocks are locally protomylonitic at distances <800 m from the AFS trace, and deformation-related magnetic anisotropy is present as far as 4–5 km from the AFS in the Cerro del Pingo pluton (Saldías et al., 2015). Gradients of decreasing fabric strain intensity both away from the AFS trace and along strike of the AFS away from synkinematic plutonism indicate that mylonitic shear required proximity to both the fault system and the magmatic thermal source, and pluton intrusion further than ~1.3 km from the AFS is marked by contact metamorphism without shear. AFS shear zones were progressively overprinted by brittle deformation as the thermal influence of plutonism waned, but sinistral shear continued, as evidenced by cataclastic overprint of mylonitic fabrics along the eastern (main) branch of the AFS and abundant ~ N–S striking sinistral faults (Seymour et al., 2020).

Regional-scale (1:100,000) geologic mapping near Taltal (Escribano et al., 2013) depicts mylonitic fabric along the eastern branch of the AFS east of Taltal, where a ~500 m wide shear zone affects the Matancilla Plutonic Complex and the Jurassic La Negra Formation. As mapped, this shear zone contradicts the model that magmatism-connected ductile deformation was limited to the Early Cretaceous, and suggests either that the AFS was active as early as the Middle Jurassic or that localized ductile deformation occurred in the Early Cretaceous independent of thermal weakening from an adjacent pluton. Outcrops of the Las Tipias granodiorite with a 139 ± 3 Ma K–Ar date (Las Cenizas, 2007 *in* Escribano et al., 2013) are mapped near the mylonite zone, and it is possible that the mapped mylonitic zone is associated with this Early Cretaceous pluton instead of the Jurassic Matancilla Plutonic Complex. We use geologic mapping, structural measurements, and microstructural observations to revise the spatial extent of the Matancilla shear zone and show that mylonitic deformation is more extensive than previously mapped and tied to intrusion of the Middle Jurassic Matancilla Plutonic Complex rather than the Early Cretaceous AFS.

3. Methods

To constrain the spatial relations, kinematics, and timing of the Matancilla shear zone, we employ 1:25,000-scale geologic mapping, petrographic analysis of ductile fabrics, and U–Pb zircon geochronology. Aureole mineral assemblages were determined using petrography and a Malvern Panalytical TerraSpec® Halo handheld spectrometer. Structural measurements are plotted using Stereonet (Allmendinger et al., 2011; Cardozo and Allmendinger, 2013), and length-weighted rose diagrams of mapped contacts are generated using the OAtools plugin for ArcGIS (Kociánová and Melichar, 2016). We utilize petrographic and outcrop kinematic indicators such as asymmetric folds, S–C fabrics, and oblique recrystallized grain shape fabric (e.g., Passchier and Trouw, 2005) for determining shear sense. U–Pb zircon analyses of a cross-cutting pluton were conducted using laser ablation inductively-coupled mass spectrometry (LA-ICP-MS) instrumentation at the UTChron laboratory at the University of Texas at Austin following methods outlined in Seymour et al. (2020). Thick sections were scanned for monazite using a TESCAN Integrated Mineral Analyzer at the Colorado School of Mines. U–Pb analyses were conducted at the University of California, Santa Barbara lab, using laser-ablation split-stream inductively coupled plasma mass spectrometry (LASS-ICPMS) following the methods of Kylander-Clark et al. (2013). Concordia diagrams and weighted mean average (WMA) calculations are generated with IsoplotR software (Vermeesch, 2018), using the 95% confidence method for WMA uncertainty calculation and filtered for ≤10% discordance.

4. Pre-mylonitic deformation recorded in the Paleozoic Chañaral Epimetamorphic Complex

The Matancilla shear zone overprints earlier deformation in the late Paleozoic Chañaral Epimetamorphic Complex metasedimentary rocks. Here we begin by characterizing the older deformation history to provide a framework for interpreting the Jurassic and Cretaceous strain. Sedimentary compositional layering is often distinguishable in non-mylonitic lower-greenschist facies quartzite and phyllite as alternating metasiltstone and metasandstone layers at millimeter to meter scales (Fig. 3). Phyllitic foliation defined by aligned fine-grained micas and pressure solution seams is most strongly developed in finer-grained protoliths and most commonly parallel to bedding. Outcrop-scale folds (Fig. 3B and C) in the Chañaral Epimetamorphic Complex deform the

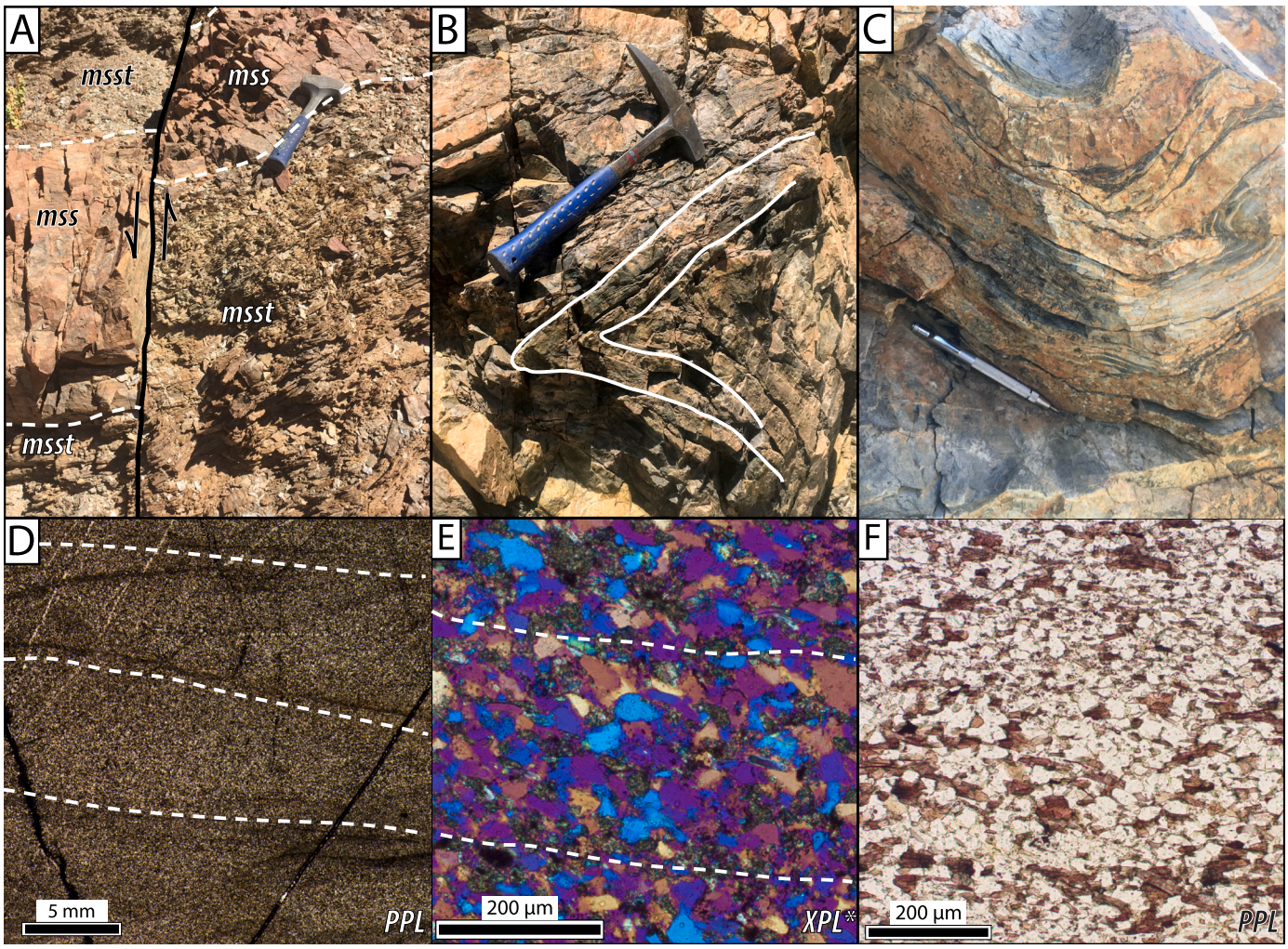

Fig. 3. Metasedimentary rocks of the Late Paleozoic Chañaral Epimetamorphic Complex. A) Nonmylonitic metasandstone (mss) and metasiltstone (msst, bedding marked by dashed white lines) displaced by a sinistral N-striking fault (solid black line) associated with the Atacama fault system. Foliation is parallel to sedimentary compositional layering. View facing north. B) Tight recumbent folding of quartzose metasandstone. C) Plunging upright open folds in quartzose metasandstone. D) Thin section photograph of nonmylonitic Chañaral Epimetamorphic Complex metasandstone >5 km away from the Matancilla Plutonic Complex intrusive contact. Faint foliation in this sample (dashed white lines) is parallel to compositional layering. E) Detail view of the sample in 3D showing foliation defined by aligned biotite (parallel to dashed white lines). F) Metasiltstone with quartz static recrystallization indicated by straight 120° grain boundaries and lack of undulatory extinction when viewed in cross polarized light. Foliation oriented parallel to Matancilla mylonitic fabrics is preserved by aligned biotite. See Fig. 2 for photo locations. PPL = plane polarized light, XPL = crossed polarized light, * = gypsum plate inserted.

foliation and record deformation that is absent in surrounding Mesozoic rocks. Isoclinal folds are not observed which suggests that the foliation represents burial metamorphism rather than transposition. Bedding most commonly dips shallowly, but meter-scale folds are sparsely present in outcrop, with at least two styles and orientations of folding recognized. A stereoplot of poles to bedding (Fig. 4A) shows a broad scattering of orientations not easily explained by a single deformation event. One outcrop exposes open, upright, folds with shallowly W-plunging fold axes (Fig. 3C, blue symbols on Fig. 4B), while another outcrop 670 m to the south is characterized by close, gently-inclined folds with S-plunging fold hinges (Fig. 3D, red symbols on Fig. 4B). Fold hinges from these two outcrops are nearly orthogonal and cannot be explained by a single cylindrical folding event. Neither fold has an associated axial planar cleavage, and field exposure did not permit a determination of the relative timing of these fold events.

Crenulation lineation is sparsely visible on foliation surfaces in phyllitic intervals. Crenulation lineation measurements, along with fold axes measured in outcrop and calculated stereographically are dominantly oriented NE-SW to N–S with shallow plunges (Fig. 4C); these orientations are different from the E-W to NW-SE trending fold axes reported by Bell (1984) between latitudes 25.5–27°S. Variation between measurements indicates that these lineations are either related to multiple deformation events or formed in one event and were rotated about a subvertical axis by subsequent deformation. In either case, structural data in this study provides evidence for at least two deformation events in the Chañaral Epimetamorphic Complex prior to the intrusion of the Matancilla Plutonic Complex, and demonstrates that these older fabrics and structures were not reactivated during Middle Jurassic shearing.

5. Geometry, kinematics, and microstructures of mylonitic fabrics associated with the Matancilla Plutonic Complex

5.1. Field relations

Our geologic mapping refines the spatial extent of ductile shear zones east of Taltal and revises the patterns of AFS-connected deformation. Mylonitic fabrics are most developed in the Paleozoic Chañaral Epimetamorphic Complex near the contact where it is intruded by the Matancilla Plutonic Complex (Figs. 2 and 5). The map pattern of the boundary between mylonitic and nonmylonitic Chañaral

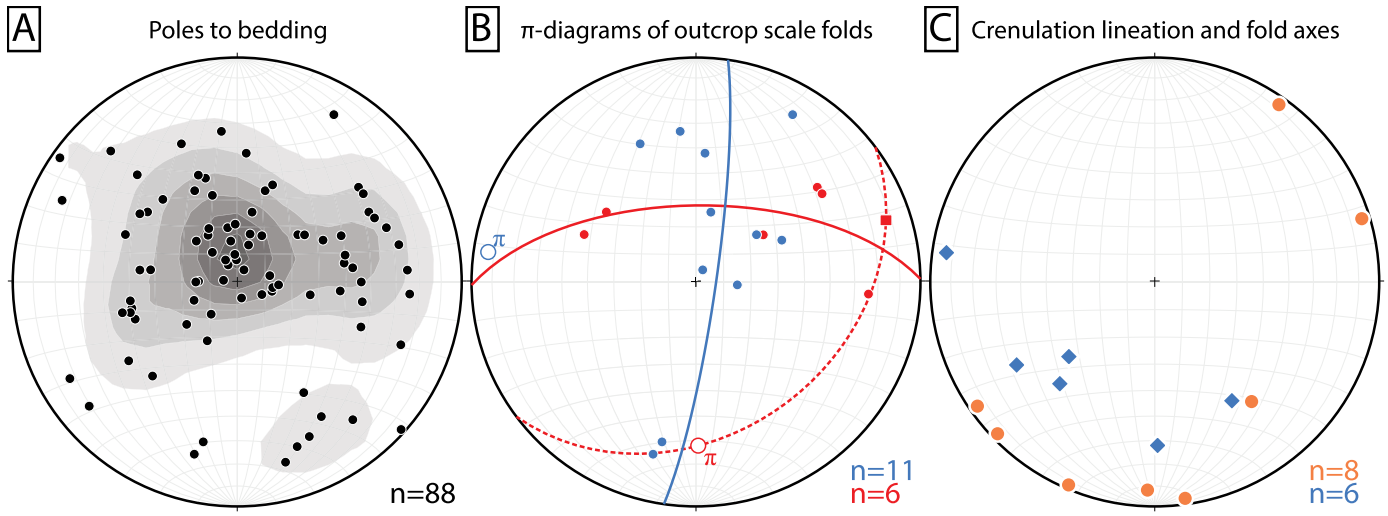

Fig. 4. Stereoplots of structural data in the Chañaral Epimetamorphic Complex metasedimentary rocks. A) Poles to bedding (smoothed contour interval = 2, significance level = 3). Scattered poles reflect the multiple folding events observed in outcrop without a unifying girdle distribution that would characterize a single folding event. Bedding most commonly dips shallowly but in places has near vertical dips. B) π diagrams of two example outcrop-scale folds ~670 m apart. The folds show nearly orthogonal calculated π axes (278/07, bedding poles in blue and 179/28, bedding poles in red). Using a linear measurement of the axial trace for the latter fold (red square) and the calculated fold axis, the axial plane for the gently inclined fold is calculated as 053, 33 SE (dashed red line). C) Linear structural elements in Chañaral Epimetamorphic Complex metasedimentary rocks. Crenulation lineation measurements (orange circles) are measured where a crenulation lineation is visible in the bedding-parallel cleavage. Fold axes (blue diamonds) were measured in outcrop or calculated from bedding measurements across outcrop-scale folds. A broad trend of NE-SW to N–S shallowly plunging lineations is present, but significant variation indicates polyphase deformation.

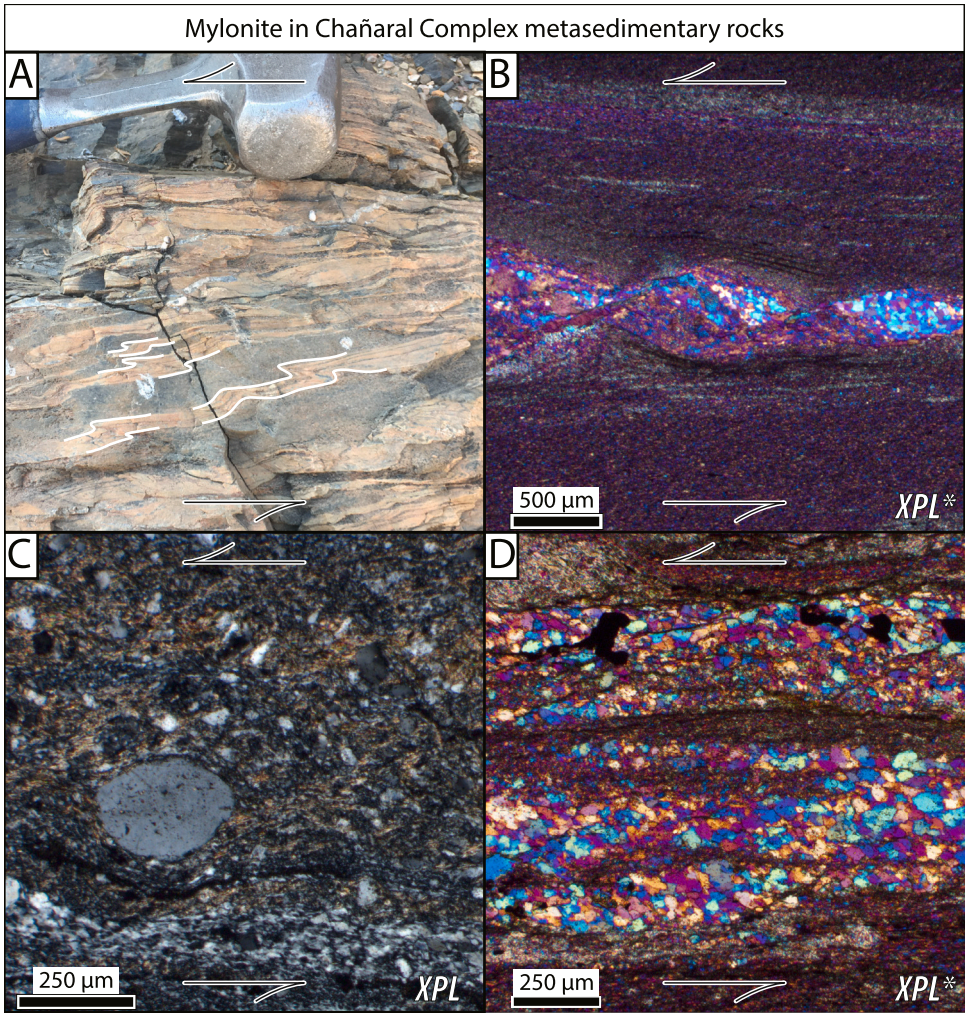

Fig. 5. Field photos and X:Z plane photomicrographs of mylonite in metasedimentary rocks in the aureole of the Matancilla pluton. A) Weakly mylonitic quartzite and phyllite of the Chañaral Epimetamorphic Complex ~400 m away from the contact with the Matancilla Plutonic Complex. Asymmetric folds (white highlight) indicate sinistral shear. Photo faces down and to the west. B) High strain mylonite in fine grained metasedimentary protolith of the Chañaral Epimetamorphic Complex, with a boudinaged quartzose layer displaced by shear bands. C) Heterogeneously-strained mylonite in a Chañaral Epimetamorphic Complex metasedimentary protolith. D) Thinly-bedded metasiltstone and metasandstone with subgrain rotation as the dynamic recrystallization mechanism in quartzose layers. Sinistral shear sense (arrows) is determined for the photomicrographs using C′ shear bands (B–D) and recrystallized quartz oblique grain shape (B, D).

Epimetamorphic Complex metasedimentary rocks roughly parallels the contact of that unit with the Matancilla Plutonic Complex to the west. Near the Quebrada Tipias fault, the northwestern boundary of the Matancilla mylonitic zone is ~630 m away from the intrusive contact, though further south weak mylonitic fabrics are found as far as 1.4 km from the contact. In areas far from the pluton with weak mylonitic deformation, the mylonitic fabric is only visible in finer-grained phyllitic intervals, while quartzose metasandstone is unstrained. This relation is disrupted by the granodioritic Las Tipias pluton, which cuts the Matancilla intrusive contact and the mylonitic fabrics in the aureole of the older pluton. East of the gradational mylonitic zone boundary, a weak cleavage is visible in fine-grained intervals of the Chañaral Epimetamorphic Complex at a high angle to bedding and parallels the mylonitic fabrics exposed further west.

At the intrusive contact with Paleozoic rocks, granodiorite of the Matancilla Plutonic Complex is locally sheared into a narrow zone of pervasive protomylonite (Fig. 6). Protomylonitic fabrics in the granodiorite are markedly less strained and encompass zones significantly thinner than the mylonitic fabrics in the surrounding metasedimentary rocks. The thickness of the protomylonitic zone is commonly 2–3 m adjacent to the contact with Chañaral Epimetamorphic Complex metasedimentary rocks but locally reaches >350 m of structural thickness south of the Quebrada Tipias fault (Fig. 2).

Away from the intrusive contact, discrete centimeter-to meter-scale mylonitic zones exist throughout the Matancilla Plutonic Complex (Fig. 7). These discrete mylonitic zones are subplanar, undulating, or anastomosing and accommodate localized strain in otherwise unstrained granodiorite. Where unstrained, the dominant Matancilla pluton lithology is hypidiomorphic granular biotite hornblende granodiorite, which grades into discrete mylonite within the span of centimeters. Discrete zones are almost always marked by localized mineral alteration and are exposed in outcrop with a bleached or pinstriped appearance (Fig. 7).

We describe details of mylonitic rocks in three categories based upon spatial relations, protolith, and style of ductile strain: (i) pervasive mylonitic fabric in the Paleozoic metasedimentary rocks spatially associated with the Matancilla Plutonic Complex intrusive contact (Fig. 5); (ii) pervasive protomylonitic fabric within the Matancilla Plutonic Complex associated with the same intrusive contact (Fig. 6); and (iii) discrete cm-scale thickness, anastomosing mylonitic zones throughout the Matancilla Plutonic Complex (Fig. 7). In contrast to previous geologic mapping, we identify a thick zone of cataclasite along the eastern margin of the AFS eastern branch but find no spatial relation of any ductile fabrics with respect to that fault.

5.2. *Mylonite in Chañaral Epimetamorphic Complex metasedimentary rocks in the Matancilla Plutonic Complex aureole*

The most extensive and most pervasively strained ductile deformation is within Chañaral Epimetamorphic Complex rocks surrounding the Matancilla Plutonic Complex, where the mylonitic zone extends as far as 1.4 km from the intrusive contact (Figs. 2 and 5). Pervasive mylonitic foliation in Chañaral Epimetamorphic Complex rocks strikes SSW and dips steeply NW on average (212, 78 NW; Fig. 8A). Where the intrusive

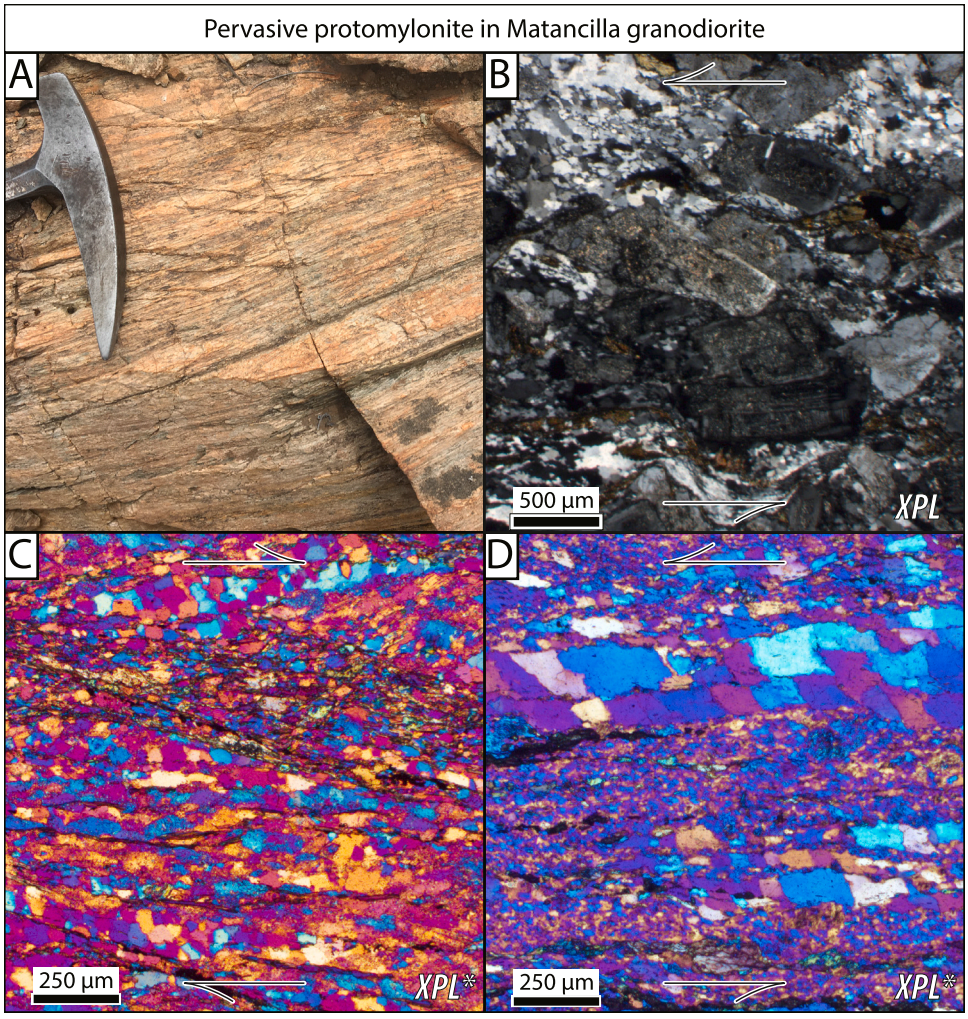

Fig. 6. Field photos and X:Z plane photomicrographs of pervasive protomylonite at the margin of the Matancilla pluton. A) Pervasive protomylonitic foliation within Matancilla Plutonic Complex granodiorite. Photo faces down and to the NW. B) Protomylonite in Matancilla granodiorite. C) Sample of pervasive mylonite near the Matancilla intrusive contact with shear bands indicating dextral shear. D) Protomylonite with grain boundary migration recrystallization mechanism textures. Large, recrystallized quartz grains envelop or are pinned against biotite. Shear sense is interpreted from C′ shear bands (B–C) and/or recrystallized quartz oblique grain shape (A, D).

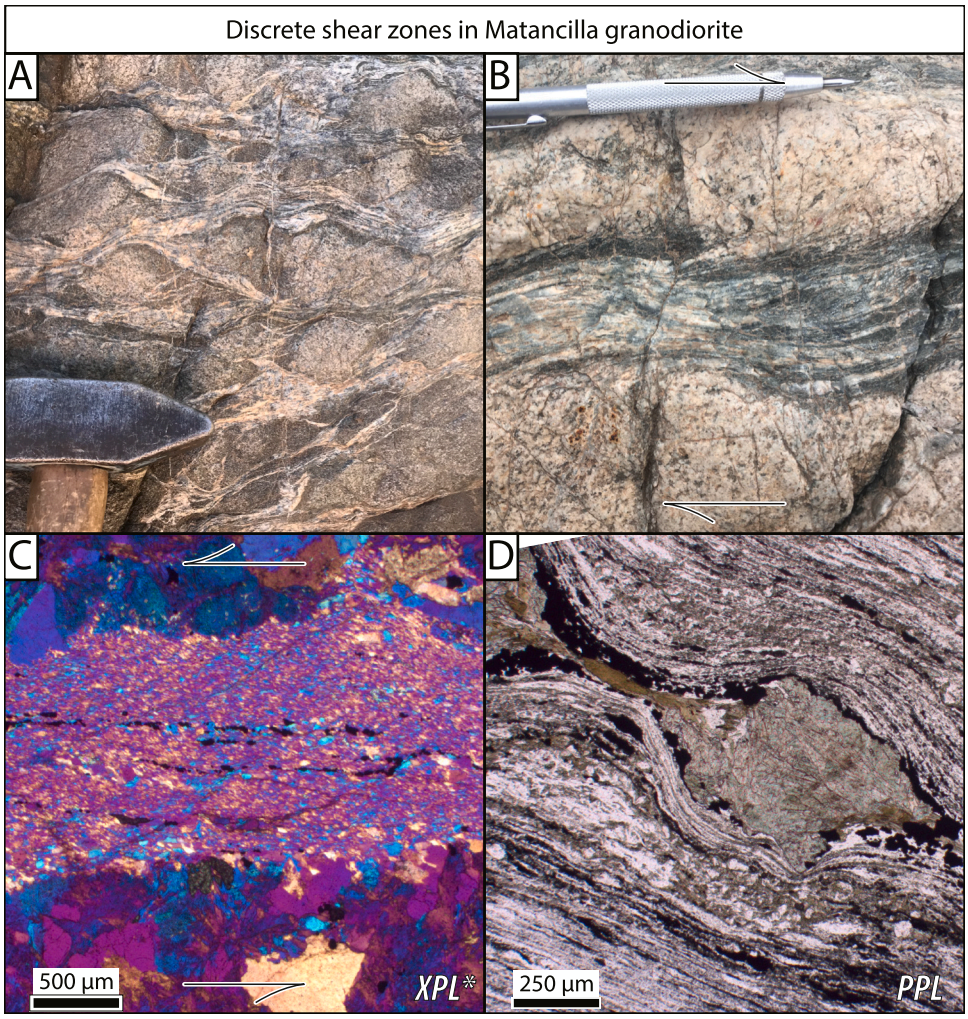

Fig. 7. Field photos and photomicrographs of discrete shear zones within the Matancilla plutonic complex. A) Anastomosing discrete shear zones in Matancilla granodiorite in a zone with unusually high density. Photo faces down and to the SE. B) Gradation from high strain ultramylonitic zone into unstrained Matancilla mylonite. Curvature of the strain fabric indicates dextral shear. Photo faces down and to the NW. C) Sharp transition from unstrained Matancilla granodiorite into an ultramylonitic quartz-feldspar discrete shear zone. Shear sense is interpreted from C′ shear bands. I) Boudinaged actinolite (green) and Fe-oxides (opaque) in ultramylonite of a discrete shear zone.

eastern contact of the Matancilla Plutonic Complex deflects across topography near the Quebrada Tipias fault the contact dips steeply northwestwards; this map pattern suggests that the mylonitic fabric is subparallel to the contact in three dimensions. Stretching lineations plunge shallowly NE or SW (average 028/05; Fig. 8A). Many outcrops have strong foliation with faint or no lineation; a lineation was measured at 41% of localities with a foliation measurement, and fabrics with lineation are commonly S > L tectonites. Foliation measurements are slightly variable and correlate with the orientation of the Matancilla intrusive contact. Bedding folded by pre-mylonitic deformation in the Chañaral Epimetamorphic Complex is transposed into parallelism with the mylonitic fabric, and there is no girdle distribution of poles to mylonitic foliation or evidence for post-mylonitic refolding. Strain degree is variable across Chañaral Epimetamorphic Complex protolith lithologies in the distal areas of the mylonitic aureole, where quartz-rich protoliths are unstrained and retain rounded detrital textures while finer-grained lithologies have protomylonitic shear fabric that was focused into these domains rich in aligned mica grains (Fig. 5C). In more highly-strained samples closer to the intrusive contact, quartz-rich horizons are dynamically recrystallized with textures indicative of subgrain rotation and bulging recrystallization mechanisms.

Asymmetric folds, S–C fabric, C' shear bands, and oblique recrystallized quartz grain shape fabric most commonly indicate sinistral shear, though dextral shear sense indicators are also observed. In the metasedimentary mylonite, petrographic shear sense determinations are sinistral in all nine oriented X:Z thin sections, though outcrop-scale shear sense indicators from locations without petrographic samples (mostly near the Quebrada Tipias fault) more commonly suggest dextral shear. Poikiloblastic andalusite is present within and slightly beyond the mylonitic envelope surrounding the Matancilla Plutonic Complex (Fig. 9), and absent in Chañaral Epimetamorphic Complex rocks away from the Matancilla aureole. Petrographically, porphyroblasts are commonly replaced by sericite-rich fine-grained mixtures and highly strained (Fig. 9C), with increasing strain in samples closer to the intrusive contact. Where strained, asymmetric σ- and δ-type pseudomorphs of andalusite porphyroclasts with quartz and white mica in pressure shadows indicate sinistral shear consistent with shear sense indicators in other phases. Elongate lenses dominated by fine-grained white mica with aspect ratios of >30:1 likely represent highly strained pseudomorphs of andalusite (Fig. 9C). Relict mylonitic foliation is preserved as aligned inclusions within andalusite and rotated within porphyroclasts to angles discordant with the surrounding ductile shear fabric (Fig. 9D). In conjunction with the spatial restriction of andalusite to the Matancilla Plutonic Complex aureole, preservation of the early-formed mylonitic fabric suggests porphyroblast development was synkinematic with shear zone development and occurred during emplacement of the Matancilla Plutonic Complex. Quartz, adularia, and chlorite veins cut mylonitic fabrics but are commonly folded, often with fold vergence consistent with other kinematic indicators, indicating veining was synkinematic or late synkinematic with ductile shear. Several samples have petrographic evidence for quartz annealing indicative of postmylonitic static recrystallization, with equant grains and straight boundaries, ~120° intergrain angles, and little to no undulatory extinction.

Microscopic postmylonitic monazite overprints Chañaral

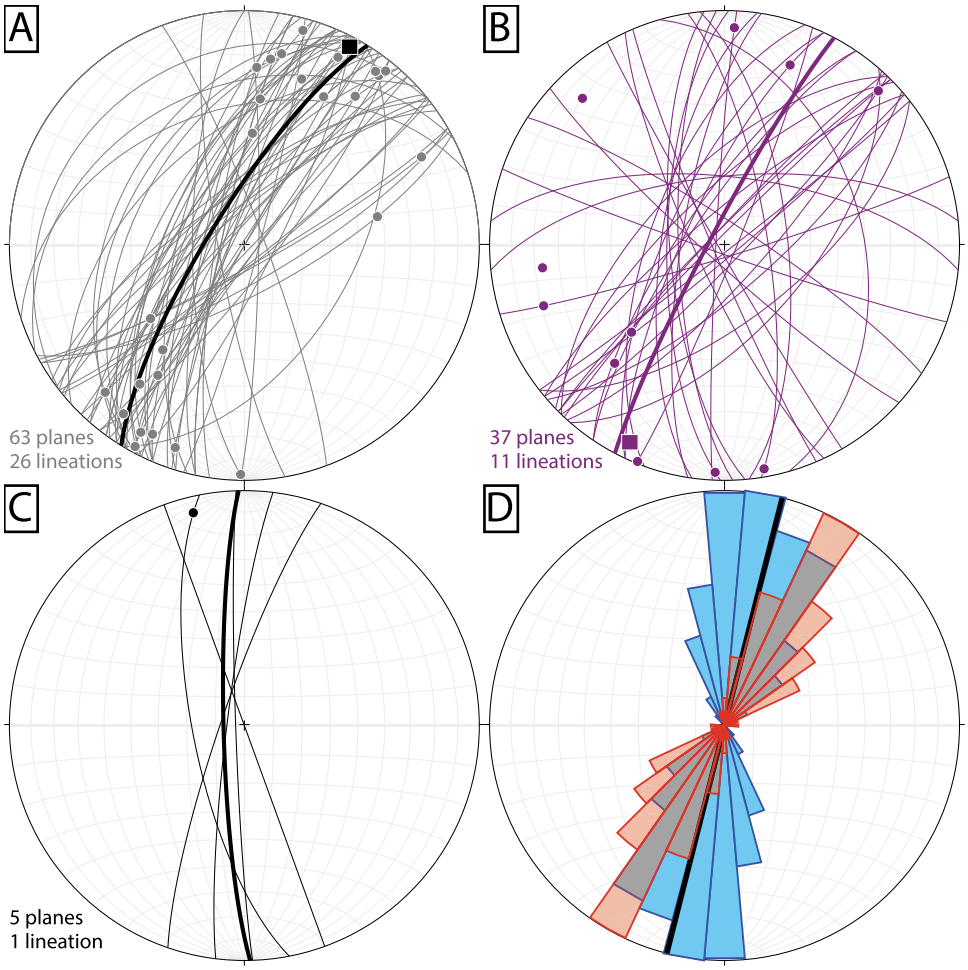

Fig. 8. Geometry of the Matancilla shear zone, with average foliation and lineation for each population plotted in bold. A) Stereoplot of mylonitic foliation and lineation in metasedimentary rocks surrounding the Matancilla Plutonic Complex. B) Discrete mylonitic shear zones from within the Matancilla Plutonic Complex. C) Stereoplot of mylonitic foliation and lineation measured in the narrow zone of pervasive protomylonite along the eastern margin of the Matancilla Plutonic Complex. D) Rose diagram showing the distance-weighted azimuthal distribution of the Matancilla Plutonic complex intrusive contact (blue) over the 9 km mapped length in 10° bins. The linear directional mean azimuth of 14° is shown with a bold line. Measured strikes of Chañaral Epimetamorphic Complex mylonitic fabric (red) are on average 18° clockwise of the intrusive contact, an obliquity consistent with sinistral shear.

Epimetamorphic Complex metasedimentary mylonite in one sample collected 150 m from the AFS (Fig. 10). Monazite grains, typically 40–50 μm in diameter, are equant and not aligned parallel to the mylonitic foliation. Relict mylonitic foliation is locally preserved within monazite grains, and the foliation is truncated at monazite grain boundaries rather than deflected around grains (Fig. 10C). Together, these textural observations support an interpretation that monazite growth postdates development of the mylonitic fabric within Chañaral Epimetamorphic Complex metasedimentary rocks.

5.3. Matancilla protomylonite

Pervasive protomylonitic fabric within the Matancilla Plutonic Complex has limited spatial extent and is restricted to the eastern margin of the plutonic complex where it intrudes the Chañaral Epimetamorphic Complex. Most exposures with this deformation style have weak planar fabric defined by aligned biotite and hornblende and recrystallized but not continuous quartz ribbons. Protomylonitic fabric in granodiorite strikes NNW to NNE and dips 83°W on average (Fig. 8C). Where the intrusive contact is exposed, protomylonitic foliation parallels the adjacent contact trace. Only a single locality has a weak but measurable linear fabric as a S > L tectonite, where the stretching lineation rakes shallowly north. In thin section, aligned mafic minerals (biotite, hornblende) and discontinuous zones of recrystallized quartz or polyphase quartz-feldspar mixtures define the protomylonitic fabric. Subgrain rotation is the most commonly observed recrystallization mechanism in quartz-rich zones. Plagioclase with partially sericitized zones forms an interconnected strong phase and lacks dynamic recrystallization textures (Fig. 6B). Microfaults demonstrate brittle behavior of feldspar and are commonly synthetic to sinistral shear sense from other kinematic indicators. Fine-grained recrystallized quartz-feldspar mixtures record the most strain, but feldspar clasts lack plastic deformation in most samples, and larger grains instead have brittle fractures. Petrographic shear sense indicators including C′ shear bands, folded chlorite and epidote veins, and oblique quartz recrystallized fabric indicate sinistral shear in 3 of 4 protomylonite oriented thin sections with shear sense determination, and one sample has C' shear band indicators for dextral shear (Fig. 6C). Secondary actinolite is locally sheared into low-strain σ-shape porphyroclasts, indicating late synkinematic fluid mobility. Late calcite veins cut the mylonitic foliation and are unstrained.

5.4. Discrete shear zones in the Matancilla Plutonic Complex

Irregularly spaced, centimeter-to meter-thick, decimeter to decameter-long discrete shear zones record localized ductile shear within the Matancilla Plutonic Complex. Discrete shear zones are gradational from unstrained granodiorite into highly strained zones over centimeters to millimeters with locally intense ultramylonitic strain (Fig. 7), with meter to decameter spacing between higher strain zones typical. The dominant interconnected weak matrix is fine-grained feldspar + quartz ± mica mixtures. Brittle shear fractures locally displace quartz and plagioclase porphyroclasts, indicating strong behavior of those phases relative to the weaker matrix assemblage. In higher-strain samples, zones of pure quartz matrix have pervasive subgrain recrystallization textures with local bulging recrystallization. Sericitized feldspar locally has minor recrystallization textures. Fine-grained mica and epidote grains are disseminated throughout the polyphase matrix in the highest strain samples.

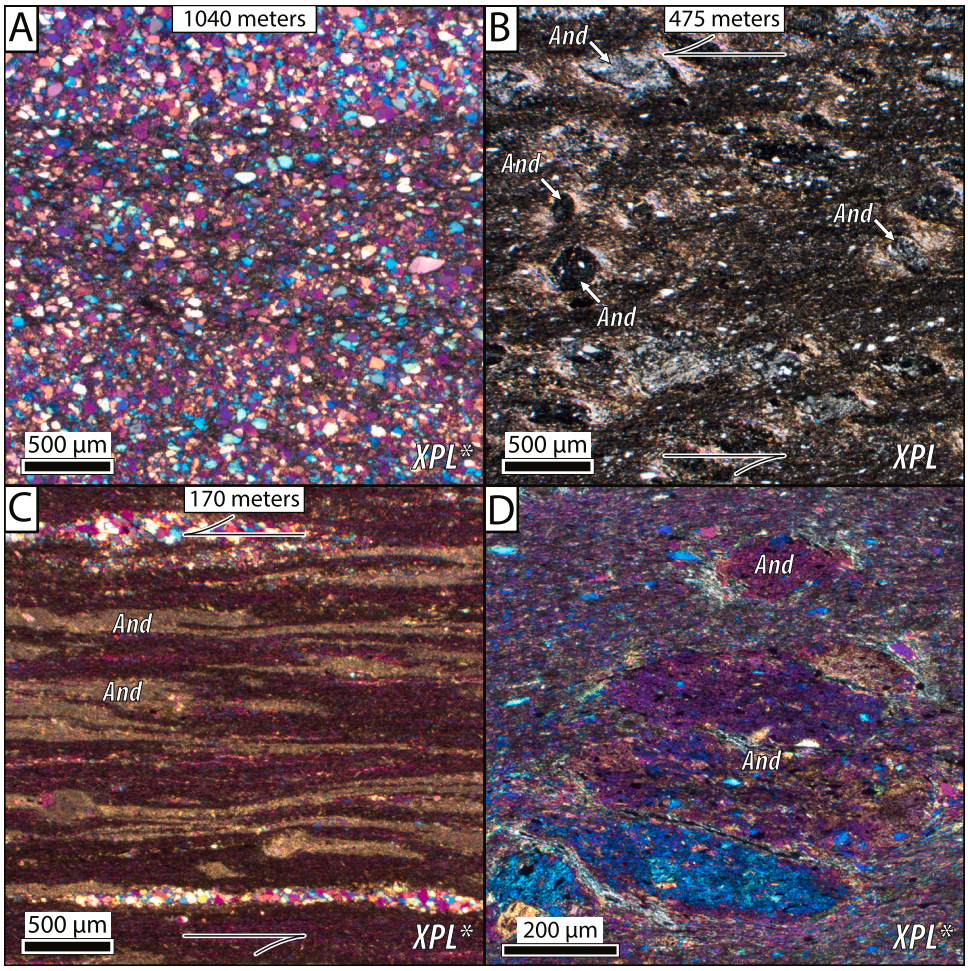

Fig. 9. Photomicrographs of Chañaral Epimetamorphic Complex metasedimentary rocks with increasing proximity to the Matancilla Plutonic Complex (distance to intrusive contact labeled). A) Nonmylonitic metasandstone outside of the mylonitic aureole lacking andalusite porphyroblasts. Bedding-parallel foliation defined primarily by dark pressure solution seams and roughly aligned fine-grained mica. Quartz has undulatory extinction and minor static grain growth but lacks dynamic recrystallization textures. B) Mylonitic metasiltstone with synkinematic andalusite porphyroblasts. Both σ- and δ-type andalusite porphyroclasts indicate sinistral shear. C) More highly strained metasedimentary mylonite with dynamic recrystallization texture of quartz and highly strained lenses of sericite-rich pseudomorphs of andalusite porphyroclasts. Oblique grain shape fabric of recrystallized quartz and σ-type andalusite pseudomorphs indicate sinistral shear. D) Detail view of poikiloblastic andalusite porphyroclasts (same sample as B), showing relict mylonitic fabric as inclusions within andalusite. And = andalusite, other abbreviations as for Fig. 3.

In contrast to the pervasive mylonitic fabrics near the margin of the Matancilla Plutonic Complex, discrete shear zones within the pluton have significant alteration and mineral replacement textures, and a pinstriped or bleached appearance in outcrop (Fig. 7). Feldspar is pervasively altered to sericite, and mafic minerals are completely chloritized. Clots of secondary actinolite form resistant boudins with biotite in boudin necks (Fig. 7D), and fine-grained actinolite is locally present along C' shear bands, indicating alteration was coeval with mylonitization. Fe-oxides, adularia, and patchy calcite are likewise involved in ductile shear fabrics, and additional generations of adularia, calcite, and chlorite veins cut the mylonitic foliation. Secondary fluid inclusions mottle quartz grains.

Discrete mylonitic foliation within the Matancilla Plutonic Complex has variable orientations but are most commonly N- to NE-striking and steeply dipping, and the average foliation is NE-striking (208, 85 NW; Fig. 8B). Eigenvalue statistics of foliation poles find subequal values between the point and girdle indices of Vollmer (1990), with a lesser random index, signifying that the distribution of mylonitic fabric is systematically scattered from a point distribution. This distribution is consistent with field observations of anastomosing and undulatory discrete shear zones. A slightly bimodal distribution of discrete shear zone foliations could alternatively reflect a scattered conjugate relation, but the lack of systematic difference of measurements with sinistral or dextral shear sense does not lend support to this interpretation. Lineations are shallowly raking (206/08 average, Fig. 8B). Only 30% of discrete mylonite foliation measurement localities have a measured lineation, though good exposures of the foliation surface are not present at every outcrop where foliation was measured, and therefore the presence of lineations may be underrepresented. Kinematic indicators for discrete shear zones are variable. Of four oriented thin sections, three indicate sinistral shear and one has mixed shear sense. Hand sample kinematic indicators along X:Z surfaces are dominantly sinistral, though dextral shear sense indicators were also observed.

6. Development of mylonitic fabrics

6.1. Shear zone kinematics

Across all protoliths, 17 thin sections yield a confident shear sense determination, and 15 of these have sinistral shear sense indicators. However, 7 of 11 shear sense indicators from outcrops without petrographic samples are dextral, indicating possible heterogeneous shear. No geometric pattern is evident that separates mylonitic foliation and lineation measurements with sinistral and dextral shear sense indicators; both are NNE-to NE-striking on average with shallowly raking lineations. Sinistral shear sense indicators are the most widespread across the shear zone, while dextral kinematic indicators are most common in the aureole between the Taltal and Quebrada Tipias faults and could reflect a localized strain anomaly or change of pluton margin geometry. Some localities have seemingly conflicting indicators for sinistral and dextral shear in outcrops separated by only tens of meters, without deflection of the mylonitic foliation. Variable shear sense indications may reflect heterogeneous rheology at meso- and micro-scales controlled by alternating quartzose and micaceous protoliths in the Chañaral Epimetamorphic Complex metaturbidites or by localized discrete shear along possible fluid pathways in the Matancilla Plutonic Complex. From the dominance of clear sinistral shear sense indicators, especially in samples where multiple phases and microstructures indicate the same

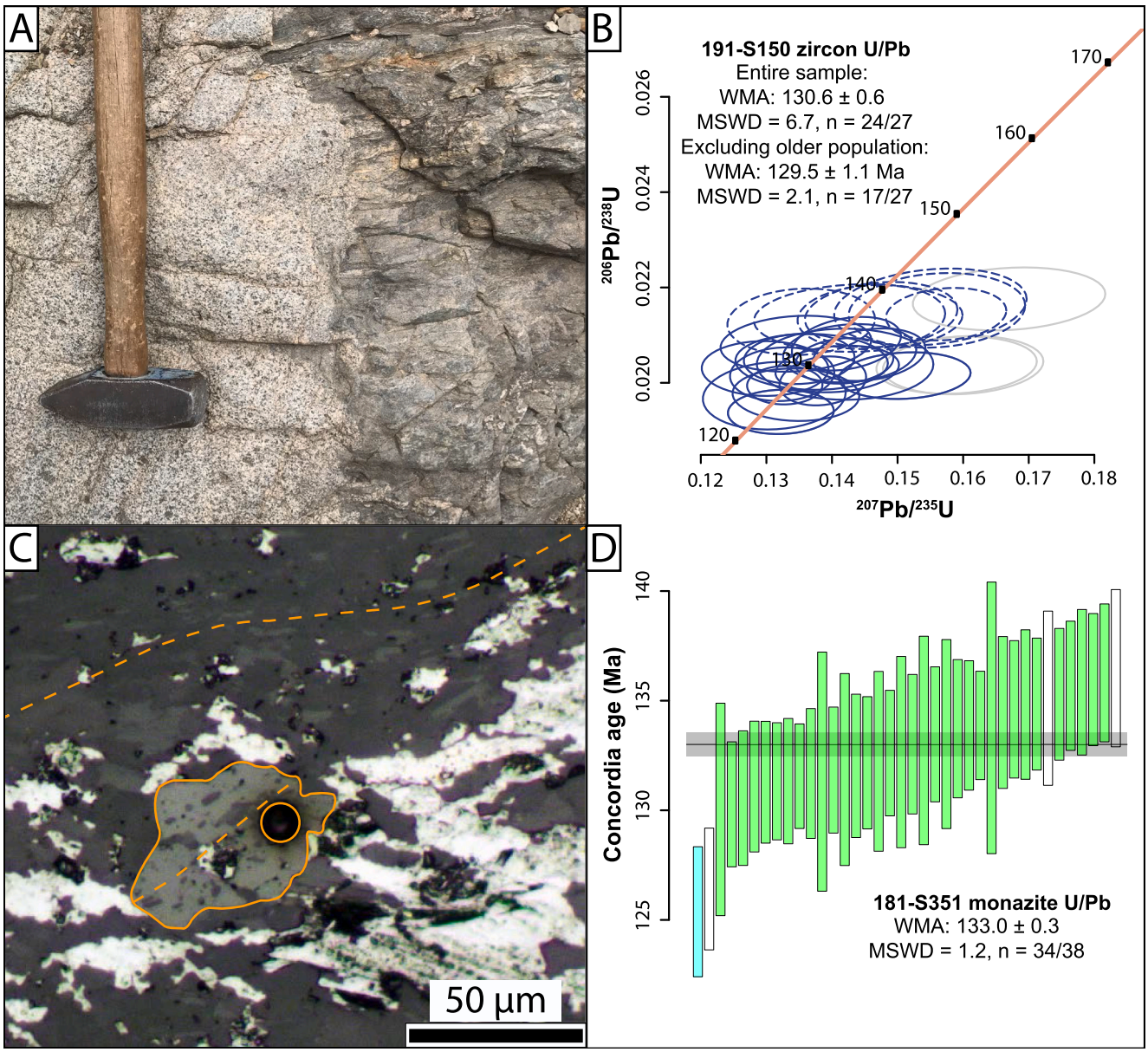

Fig. 10. Crosscutting relationships and geochronology of Early Cretaceous features that postdate the Matancilla shear zone. Sample locations are referenced in Fig. 2. A) Intrusive contact of the Las Tipias granodiorite cross-cutting the mylonitic fabric in metasedimentary rocks in the aureole of the Matancilla Plutonic Complex. The Las Tipias granodiorite is unstrained at the contact. B) U–Pb concordia diagram for a sample from the Las Tipias granodiorite. Data-point error ellipses are 2σ. Gray ellipses show analyses with >10% discordance excluded from calculations. Dashed ellipses mark concordant analyses that possibly represent an older zircon population. C) Reflected light photomicrograph of a monazite grain (yellow outline) within a sample of Chañaral Epimetamorphic Complex metasedimentary mylonite. The dashed yellow line traces foliation in the mylonite, and relict mylonitic foliation included within the postkinematic monazite. The outlined circle marks an ablation pit created during analysis of the monazite grain. D) Plot of monazite U–Pb dates with 2σ uncertainty. Hollow symbols indicate excluded analyses with >10% discordance, and the blue symbol is an outlier omitted by the weighted mean age calculation.

shear sense, we interpret the Matancilla shear zone to record overall sinistral shear. This interpretation is also supported by the geometry of mylonitic fabrics with respect to the shear zone margin. The intrusive contact of the Matancilla Plutonic Complex largely defines the margin of the main shear zone and strikes N- to NNE-with a distance-weighted trace azimuth of 14° (Fig. 8D). On average, fabric in the Chañaral Epimetamorphic Complex mylonite aureole strikes NNE ~18° clockwise of the intrusive contact, and this obliquity is consistent with sinistral shear. The presence of S > L and S-tectonite fabrics and evidence for coaxial or antithetic (dextral) shear in parts of the shear zone suggests an overall transpressional regime with a component of shortening across the shear zone (e.g., Sanderson and Marchini, 1984).

6.2. Rheology and shear zone deformation conditions

The degree of mylonitic strain in the Matancilla shear zone is influenced by protolith lithology, proximity to the pluton thermal source, and hydrothermal alteration. The least intensely strained fabric belongs to the domain of pervasive protomylonitic granodiorite at the eastern margin of the Matancilla Plutonic Complex, where interconnected zones of recrystallized material are uncommon. Hydrothermal alteration in this domain is minor, with incompletely chloritized mafic minerals and only partial sericitization of feldspar grains. Quartz has subgrain rotation recrystallization textures, but the 20–25% modal quartz is not sufficiently strained to form a throughgoing fabric, and more abundant feldspars record entirely brittle deformation in most strained samples.

Strain intensity within the Chañaral Epimetamorphic Complex metasedimentary rocks is dependent on both lithology and proximity to the plutonic complex. In distal parts of the Matancilla shear zone, quartzose sandstone protoliths retain equant grain shapes while adjacent metasiltstone is more highly strained, and in the proximal shear zone, both protolith lithologies record plastic strain (Fig. 9). Sinistral shear in very fine-grained lithologies is likely accommodated by diffusion creep mechanisms such as grain boundary sliding and dissolution-precipitation creep, while mica-rich domains likely record slip on basal planes. Ultramylonite in the aureole is only present in the finer-grained lithology, where micaceous horizons had lower resistance to deformation.

Inclusion trails of quartz and aligned micas preserve relict mylonitic foliation within andalusite, and the restricted spatial nature of both the mylonitic fabric and of andalusite porphyroblasts to the aureole of the Matancilla Plutonic Complex provide a confident interpretation that andalusite was synkinematic with mylonitic shear. Andalusite porphyroblast growth can increase viscosity of metapelitic rocks, even to the point such that they can be stronger than metapsammitic interbeds (with sufficiently low initial effective viscosity contrast; Groome et al., 2006). However, replacement of andalusite by sericite-rich alteration products is observed in more highly-strained samples (Fig. 9), and this alteration counteracted the porphyroblast strengthening effect. Highly-strained andalusite pseudomorphs in pelitic horizons of a sample with low-strain metasandstone horizons indicates the viscosity contrast focused strain into the weaker finer-grained protoliths even where andalusite porphyroblasts are present.

The kilometer-thick zone of mylonitic fabric in Chañaral Epimetamorphic Complex metasedimentary rocks is the most extensive and has the highest strain fabrics in the Matancilla shear zone, excluding the spatially-limited discrete shear zones within the pluton. The limited ability of the unaltered Matancilla granodiorite protolith to undergo significant plastic strain reflects the much greater strength of this feldspar-rich lithology relative to the quartzose and pelitic protolith mylonitic envelope that surrounds the pluton and demonstrates that, like AFS shear zones, pelitic horizons in the thermal aureole of Middle Jurassic synkinematic plutonism were the weak link in the rheologic system and accommodated the greatest strain.

Across all mylonite protolith domains, subgrain rotation is the dominant quartz recrystallization mechanism with lesser bulging recrystallization, and these textures are consistent with mid-to upper-greenschist facies recrystallization temperatures at typical shear zone strain rates and water contents (e.g., Stipp et al., 2002; Law, 2014). Biotite and actinolite synkinematic with plastic deformation are further supportive of greenschist-facies deformation. Spectral and petrographic analysis indicates biotite and muscovite are present in Chañaral Epimetamorphic Complex rocks outside of the Matancilla aureole, but that pyrophyllite is absent. Aureole reactions that form andalusite without garnet or staurolite suggest relatively low reaction pressures of $<\sim$3 kbar and upper-greenschist facies temperatures (e.g., Pattison and Spear, 2018), which is broadly consistent with Al-in-hornblende barometry estimates of 1.9–2.4 kbar intrusion pressures for plutons in the Coastal Cordillera (Dallmeyer et al., 1996). In pure quartz domains in three samples (two metasedimentary mylonites and one Matancilla granodiorite mylonite), we estimate root mean square dynamically recrystallized quartz grain size of ~18–20 μm, suggesting differential stress of ~60–70 MPa according to the Stipp and Tullis (2003) piezometer.

Quartz static recrystallization textures overprint some Chañaral Epimetamorphic Complex mylonite samples, including a metasiltstone with aligned biotite and relict S–C fabrics located between the Las Tipias and Matancilla granodiorites (Fig. 3F). Early Cretaceous intrusion of the Las Tipias granodiorite is likely responsible for static recrystallization in samples adjacent to that pluton, but quartz static recrystallization textures present in samples within the Matancilla aureole but >5 km from the Las Tipias granodiorite suggest that Middle Jurassic deformation waned before elevated temperatures from Matancilla magmatism relaxed below quartz plasticity thresholds. In other samples, quartz veins that cut mylonitic fabrics are asymmetrically folded and recrystallized with grain boundary migration textures, consistent with high temperature and/or low strain rate deformation. A sample of a pervasively-strained granodiorite from the Matancilla Plutonic Complex near the intrusive contact has grain boundary migration dynamic recrystallization textures with 100–200 μm quartz grains that envelop or terminate against platy biotite (Fig. 6D), with a weak oblique quartz grain-shape fabric that indicates sinistral shear. Quartz grain boundary migration textures could record low strain rates in the late stages of deformation in the Matancilla Plutonic Complex thermal aureole.

Strongly heterogeneous deformation of Matancilla shear zone mylonites indicates that strain preferentially localized in weakened zones. The most highly strained domains are discrete shear zones with fine-grained feldspar + quartz-rich mixtures with pre-to synkinematic alteration phases (chlorite, actinolite, adularia, Fe-oxides, calcite, and secondary micas), and fine-grained polyphase mixtures can have the weakest rheology in quartzofeldspathic ultramylonites (Stenvall et al., 2019). Fractured quartz porphyroclasts with undulatory extinction in samples with fine-grained quartz-feldspar mixtures indicate relatively strong behavior of quartz compared to the polyphase matrix. Alteration associated with high-strain ultramylonites in the otherwise rheologically-strong granodiorite suggests that reaction softening and hydrolytic weakening allowed breakdown of strong feldspars and enhanced plastic deformation. The degree of feldspar sericitization and chloritization of mafic minerals is notably greater in high-strain discrete shear zones than in the domain of pervasive protomylonite, despite the same granodiorite protolith. Mobile fluids were likely derived either from mineral reactions (e.g., andalusite formation) or fluids associated with magmatism, and synchronous development of the discrete shear zones with pluton emplacement suggests the latter at least partly enhanced ductile strain.

6.3. Timing

The spatial pattern of the mylonitic zone in the Chañaral Epimetamorphic Complex following the intrusive contact strongly indicates that the shear fabric formed in the thermal aureole of the Matancilla Plutonic Complex. Protomylonitic fabric within granodiorite at the margins of the plutonic complex largely parallels the intrusive contact and is oriented similar to mylonitic foliation in the surrounding metasedimentary rocks, indicating that ductile shear in both domains was related to Middle Jurassic pluton emplacement.

Some discrete mylonitic fabric measurements strike roughly parallel to the AFS and have shallowly-raking lineations and sinistral shear sense indicators, which is kinematically compatible with the documented Early Cretaceous shear on the N-striking AFS (e.g., Seymour et al., 2021). However, the discrete mylonitic zones seem evenly distributed within the Matancilla Plutonic Complex and do not reflect any clear pattern of abundance or thickness with proximity to the eastern (main) branch of the AFS, and some of the discrete mylonitic foliation planes near the AFS are nearly perpendicular to the AFS strike. We find no evidence that the discrete mylonitic zones in the Matancilla Plutonic Complex are spatially or temporally connected to the AFS, and the presence of both mylonitic and nonmylonitic Matancilla granodiorite clasts in AFS cataclasite show a clear overprinting relation of AFS brittle deformation on ductile shear fabrics. Likewise, discrete shear zones are found only within the Matancilla Plutonic Complex and do not show a spatial pattern with relation to the intrusive contact of the unstrained Early Cretaceous Las Tipias granodiorite, which cuts the mylonitic fabric developed in the aureole of the Matancilla Plutonic Complex. Despite the higher orientation variability, discrete shear zones in granodiorite are, on average, similarly oriented to the mylonitic fabric in the Matancilla aureole. The average foliation measurements of discrete shear zones and mylonite in the metasedimentary aureole are only 8°

different, and the average lineations are within 13°. From the similarity in orientation and kinematics and lack of discrete shear zones overprinting pervasive mylonite, we here infer that all three mylonitic domains are temporally and kinematically connected.

The Matancilla shear zone studied here tracks along the intrusive contact of a granodiorite facies of the Matancilla Plutonic Complex with a zircon U–Pb date of 169.0 ± 1.6 Ma (Mavor et al., 2020), which we interpret as the best estimate for timing of shear zone formation. Further constraints are found from plutons that cut ductile shear fabrics. Two dates of fine-to medium-grained unstrained San Ramon granite that cross cut discrete shear zones overlap at ~160 Ma (Seymour et al., 2021). A new U–Pb zircon date of Las Tipias granodiorite, which cuts metasedimentary mylonite and lacks internal discrete shear zones, has an overall weighted mean age of 130.6 ± 1.6 (MSWD = 6.7, Fig. 10B, supplementary dataset A). A grouping of 135–137 Ma grains is discontinuous with the age spread of other grains in the sample and may represent an older population of ante- or xenocrystic grains that contribute to the high MSWD value. Excluding these grains gives a calculated WMA of 129.5 ± 1.1 (MSWD = 2.1); this is our preferred age, as the lower MSWD indicates a higher likelihood that the analyses are from a single population. In either case, the zircon data indicate the Las Tipias granodiorite is ~10 Myr younger than suggested by K–Ar methods (Escribano et al., 2013), and that Matancilla shear zone fabrics had clearly formed prior to the mid-Early Cretaceous. U–Pb dating of monazite grains that overprint Matancilla mylonitic fabric adjacent to the AFS yields a weighted mean age of 133.0 ± 0.3 Ma (MSWD = 1.2, Fig. 10B, supplementary dataset A) and a Tera-Wasserburg intercept age of 132.6 ± 0.7 (MSWD = 2.3; including all 38 analyses), confirming that the mylonitic fabric in Chañaral Epimetamorphic Complex metasedimentary rocks formed prior to the Early Cretaceous.

7. Partitioning during Jurassic oblique convergence

7.1. Mylonite as a record of regional tectonic stresses

The spatial association of mylonitic fabrics with the Matancilla Plutonic Complex intrusive contact indicates that ductile deformation occurred only where the thermal influence of plutonism weakened the surrounding quartz- and mica-rich rocks, which were weaker than feldspar-rich plutonic lithologies, but this relation alone does not determine if strain fabric reflects regional tectonism or localized transient stresses due to pluton emplacement. Matancilla shear zone fabrics satisfy two of the three strongest lines of evidence put forward by Paterson et al. (1989) to determine syntectonic pluton intrusion: (1) solid-state deformation fabric within the pluton and in the surrounding aureole parallels the intrusive contact (Fig. 8), and (2) porphyroblasts restricted to the contact metamorphic aureole are synkinematic with this fabric (Fig. 9). The third criterion, requiring parallelism of magmatic flow fabrics with solid-state deformation, cannot be evaluated as a magmatic or submagmatic foliation is not observed in the Matancilla granodiorite, and the pluton is texturally isotropic where unaffected by mylonitic shear. These criteria, along with the overall consistency of NNE-striking mylonitic foliation without any major deflections and kilometer-scale shear zone thickness suggests that ductile fabrics record regional tectonism rather than a localized strain field.

7.2. Was there a Jurassic precursor to localization of the AFS?

Observation of Early Jurassic ductile shear zones with sinistral shear sense have led some studies to posit that the main Early Cretaceous phase of AFS deformation was preceded by sinistral and/or extensional shear in the Jurassic (Scheuber and Andriessen, 1990; Scheuber and Reutter, 1992; Ring et al., 2012). The refined spatial extent and cross-cutting relations of ductile shear zones presented here show that AFS deformation near the Matancilla Plutonic Complex is exclusively brittle with cataclastic overprint of ductile fabrics. The 20–25° counterclockwise oblique angle of the AFS with the Matancilla intrusive contact and even greater obliquity to the average mylonitic foliation, along with the lack of any deflection in the straight AFS fault trace, demonstrates that Matancilla fabrics had no apparent influence on fault localization during Early Cretaceous deformation. Instead, the trace of the AFS was controlled by thermally-weakened shear zones associated with synkinematic plutonism that were linked via brittle faults to form the throughgoing fault system (Seymour et al., 2020, 2021). Intrusion of the Las Tipias granodiorite at 130 Ma is ~6 Myr later than most of the mylonitic deformation on the southern Paposo segment (Ruthven et al., 2020) and ~3 Myr later than the initiation of mylonitic deformation on the northern El Salado segment at the Cerro del Pingo pluton (Seymour et al., 2021); the latter may have been responsible for growth of ~133 Ma postkinematic monazite in the Matancilla shear zone. The AFS might have already been established as a weak brittle fault near Taltal by the time of Las Tipias intrusion, and it was likely rheologically favorable for strain to localize in the existing fault zone rather than in the pluton ≥1 km to the east.

Our findings are consistent with the hypothesis that the Early Cretaceous AFS was preceded by Jurassic deformation that likewise accommodated partitioned sinistral shear from oblique subduction into the magmatic arc, where the rheologic influence of magmatism facilitated ductile shear, as has been suggested for other syn-plutonic Jurassic shear zones (e.g., the Early Jurassic Flamenco pluton; Rodríguez et al., 2021). However, the unique setting of the Matancilla shear zone in an area where Jurassic and Early Cretaceous strike-slip systems spatially overlap allows us to determine that such shear fabrics formed in the Jurassic were not reactivated to accommodate Early Cretaceous strain. Evidence presented here does not support the notion that synplutonic Jurassic shear zones formed a throughgoing proto-AFS precursor structure that guided later strain localization. Instead, the AFS connected the thermally-weakened zones between synkinematic Early Cretaceous plutonism (e.g., between the Cerro del Pingo pluton and southern Paposo segment), independent of Jurassic shear zone geometry. Matancilla sinistral shear may reflect similar plate boundary slip partitioning as models of the Early Cretaceous AFS, and suggests that Middle Jurassic upper plate deformation was oblique with a strike-slip component.

7.3. Implications for early Andean plate reconstructions

Steeply dipping foliation and subhorizontal lineations in the Matancilla shear zone contrast with the patterns of pluton emplacement into extensional roof-uplift shear zones in the Late and Early Jurassic and contradicts suggestions that pluton emplacement only occurred when extensional fault systems were active (Grocott et al., 1994; Grocott and Taylor, 2002). Despite the dominant record of margin-perpendicular extension such as steady sedimentation in the back-arc, syndepositional normal faults in arc clastic strata, and synplutonic extensional shear zones (e.g., Grocott et al., 1994b; Scheuber and Gonzalez, 1999; Charrier et al., 2007), additional lines of evidence suggest sinistral shear in the Jurassic Coastal Cordillera could be a product of sinistral oblique plate convergence (Fig. 11). Early Jurassic sinistral shear is recognized during the emplacement of the Flamenco Pluton (Rodríguez et al., 2021). The Tigrillo fault system, which records either Early Jurassic extension (Grocott and Taylor, 2002) and/or Early Jurassic sinistral transpression (Contreras et al., 2013) is cut by a system of NW-striking sinistral faults near Cifuncho (~25.7–25.9°S). These faults appear to die out into the upper La Negra Formation, constraining faulting to before the early Late Jurassic (Contreras et al., 2013), apparently contemporaneous with intrusion of the Matancilla Plutonic Complex. NE-striking folds and thrusts south of Taltal and at ca. 22°45′S, along with discrete shear zones in the Bolfin Complex near 24°S, are compatible with NW-SE shortening and sinistral subduction obliquity in the Late Jurassic between 155 and 150 Ma (Scheuber and Gonzalez, 1999).

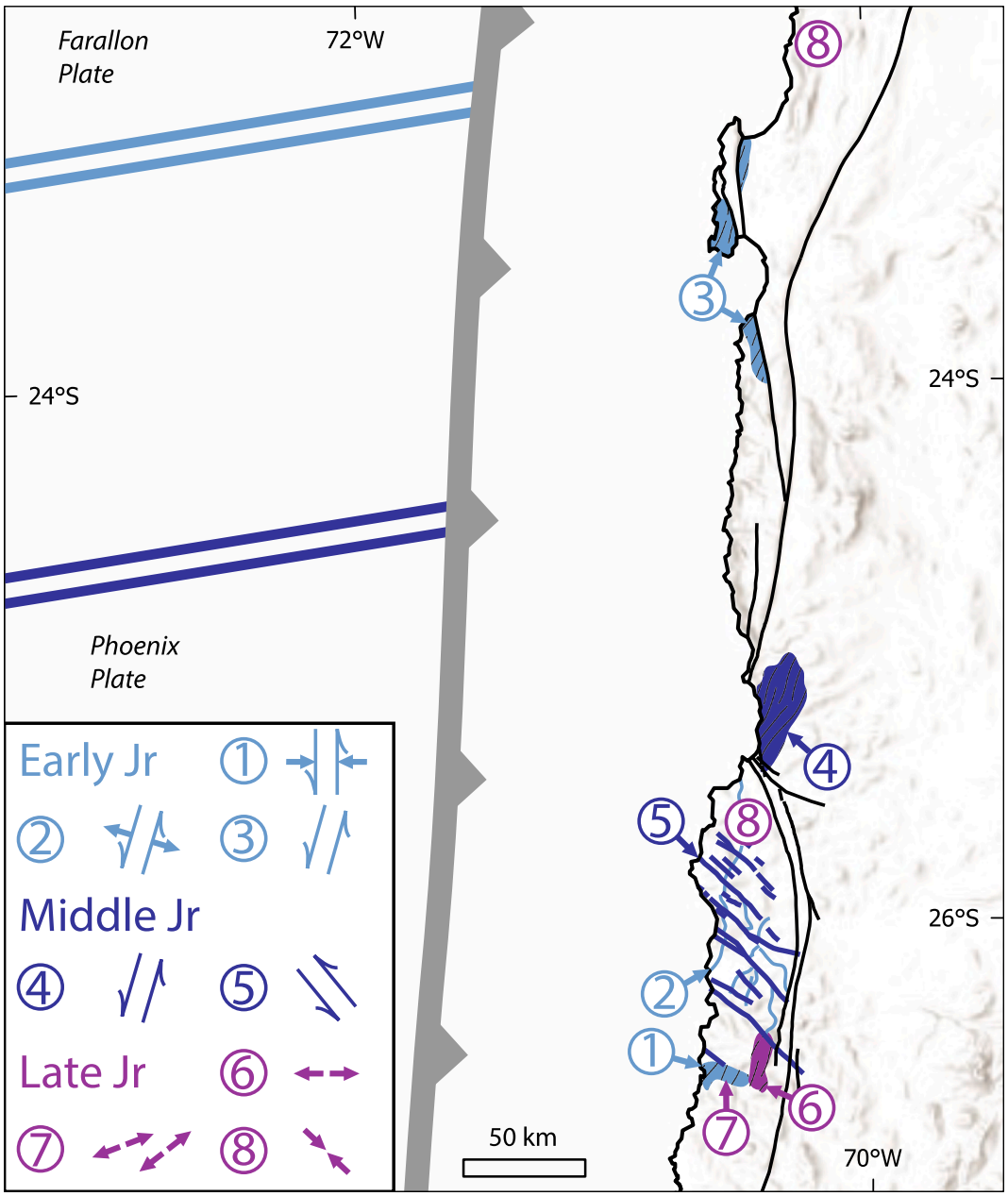

Fig. 11. Compiled lines of structural evidence for Jurassic upper plate sinistral and extensional shear in the Coastal Cordillera of northern Chile. Structures are shown schematically and have not been palinspastically restored. Legend symbols depict inferred shear sense or shortening/extension directions and are colored according to deformation timing. Positions of the Phoenix-Farallon spreading center are shown at the furthest southward positions that would impart sinistral obliquity to the northernmost onshore contemporaneous structures. The spreading center would be north of the figure area during the Late Jurassic and Early Cretaceous. Numbered structures are: 1) Sinistral shear during emplacement of the Early Jurassic Flamenco pluton (Rodríguez et al., 2021); 2) The Early Jurassic Tigrillo fault zone, recording either extensional (Grocott and Taylor, 2002) or sinistral transpressive (Contreras et al., 2013) strain; 3) Amphibolite-facies mylonitic fabric with sinistral shear sense indicators in the Bolfin Complex (Scheuber et al., 1995; Scheuber and Gonzalez, 1999); 4) The Middle Jurassic sinistral Matancilla shear zone (this study); 5) Middle or early Late Jurassic NW-striking faults near Cifuncho (Contreras et al., 2013); 6) Extension during the Late Jurassic intrusion of the Las Animas pluton (Dallmeyer et al., 1996; Grocott and Taylor, 2002); 7) Late Jurassic extension directions from dikes in the Remolino Plutonic Complex (Taylor and Randall, 2000) at 155 Ma (left) and 144 Ma (right); 8) Thrust faults and folds that developed between 155 and 150 Ma (Scheuber and Gonzalez, 1999).

Sinistral shear on the Middle Jurassic NW-striking faults near Cifuncho is compatible with the Matancilla shear zone if the regional σ_1 trended between 118° (perpendicular to the average Matancilla mylonite strike) and 138° (approximate strike of NW-striking faults), which would be required to impart sinistral shear on both structures simultaneously. While such interpretations can be complicated by stress refraction and strain partitioning, these structures provide an opportunity to fill the Middle Jurassic gap of plate-margin kinematic constraints, and contrast with suggestions that Jurassic plate convergence was entirely perpendicular to the plate boundary (Dallmeyer et al., 1996) or that onshore deformation was purely margin-normal (Scheuber and Gonzalez, 1999).

If the sinistral shear recorded by Matancilla mylonites does indeed record partitioning of oblique subduction shear into the contemporaneous magmatic arc, it would suggest that the Phoenix-Farallon-Gondwana plate triple point was north of ~25° S at 169 Ma (Fig. 11). Reconstructions showing NE-directed plate motion of the Farallon plate against the stalled Gondwana plate in the Middle Jurassic (e.g.,

Matthews et al., 2016) would impart a dextral shear sense to the margin-parallel component of partitioned strain, while the SE-directed vector of the Phoenix plate is consistent with sinistral shear. With indications for sinistral shear in the Early, Middle, and Late Jurassic, it is possible that the Phoenix-Farallon spreading center was never south of latitude 25°S through the entirety of the Jurassic, and perhaps not south of 24°S if Early and Late Jurassic margin-parallel sinistral shear in the Bolfin Complex reflects subduction obliquity (Scheuber and Gonzalez, 1999, Fig. 11). Our compilation of the structural record of onshore deformation agrees with the geochemical record (e.g., Oliveros et al., 2020) in that both datasets lack evidence of a subducting ridge passing latitude ~25°S in the Jurassic.

8. Conclusions

Mylonitic deformation associated with intrusion of the Matancilla Plutonic Complex provides a rare opportunity to constrain the Middle Jurassic tectonics of the Chilean Coastal Cordillera and challenges the paradigm that strain in the upper plate of the Andean Orogeny was exclusively extensional for most of the Jurassic. The spatial and textural characteristics of mylonitic fabrics demonstrate that ductile shear was guided by the thermal influence of the ~169 Ma Matancilla Plutonic Complex and meets the requisite timing and kinematic criteria to interpret regional strain fields from an intrusion-associated shear zone. U–Pb dates of a ~130 Ma postmylonitic intrusion and ~133 Ma post-kinematic monazite in mylonitic metasedimentary rocks show that the Matancilla shear zone predates the Early Cretaceous Atacama fault system and associated plutonism. Sinistral shear with a component of flattening strain in the NNE-striking Matancilla shear zone contrasts with the dominantly E-W extensional strain regime indicated by most Early and Late Jurassic structures. Like ductile fabrics documented for the Early Cretaceous AFS, the Matancilla shear zone may record partitioning of the strike-slip component of plate margin obliquity into rheologic weak zones in the Andean arc, but the Middle Jurassic shear zone did not serve as precursor structure to the Early Cretaceous AFS. Coupled with other work on structures compatible with Jurassic sinistral oblique convergence, sinistral shear at the Matancilla shear zone may suggest that the Phoenix-Farallon spreading center intersected the Andean trench north of latitude 25° S in the Middle Jurassic.

CRediT authorship contribution statement

S. Mavor: Writing – original draft, Project administration, Methodology, Investigation, Funding acquisition, Formal analysis, Data curation, Conceptualization. **J. Singleton:** Writing – review & editing, Project administration, Methodology, Investigation, Funding acquisition, Conceptualization. **G. Heuser:** Writing – review & editing, Investigation. **R. Gomila:** Writing – review & editing, Investigation. **N.M. Seymour:** Writing – review & editing, Investigation, Funding acquisition. **S. Williams:** Investigation. **G. Arancibia:** Writing – review & editing, Investigation.

Declaration of competing interest

The authors declare that they have no known competing financial interests or personal relationships that could have appeared to influence the work reported in this paper.

Data availability

Data will be made available on request.

Acknowledgements

Funding for this project was provided by National Science Foundation grant 1822064 to J. Singleton, a Geological Society of America student research grant to S. Mavor, and National Science Foundation EAR-PF grant 1952764 to N. Seymour. We are grateful to the University of Texas at Austin and University of California Santa Barbara labs for providing analyses and the Colorado School of Mines for instrument access. We thank Micah Hernandez and Gabriela Bórquez for field assistance. We thank two anonymous reviewers for comments that improved the manuscript.

Appendix A. Supplementary data

Supplementary data to this article can be found online at https://doi.org/10.1016/j.jsames.2022.104047.

References

Allmendinger, R.W., Cardozo, N., Fisher, D.M., 2011. Structural Geology Algorithms: Vectors and Tensors. Cambridge University Press, Cambridge, UK, p. 302. https://doi.org/10.1017/CBO9780511920202.

Álvarez, J., Jorquera, R., Miralles, C., Padel, M., Martinez, P., 2016. Cartas Punta Posallaves y Sierra Vicuña Mackenna, Región de Antofagasta. Servicio Nacional de Geología y Minería: carta Geológica de Chile. Serie Geología Básica 183–184, 147 scale 1:100,000 p. text.

Arabasz, W.J.J., 1971. Geological and Geophysical Studies of the Atacama Fault Zone in Northern Chile [Ph.D. Thesis]. Pasadena, California Institute of Technology, p. 264.

Arévalo, C., 2005. Carta Copiapó, Región de Atacama: servicio Nacional de Geología y Minería, Carta Geológica de Chile. scale 1:100,000, 1 sheet Serie Geología Básica 91, 54. p. text.

Bell, C.M., 1984. Deformation produced by the subduction of a Palaeozoic turbidite sequence in northern Chile. J. Geol. Soc. 141, 339–347. https://doi.org/10.1144/gsjgs.141.2.0339.

Bell, C.M., 1982. The lower paleozoic metasedimentary basement of the coastal ranges of Chile between 25° 30'and 27° S. Rev. Geol. Chile 17, 21–24.

Brown, M., Diáz, F., Grocott, J., 1993. Displacement history of the Atacama fault system 25°00′S-27° 00′S, northern Chile. GSA Bulletin 105, 1165–1174. https://doi.org/10.1130/0016-7606(1993)105<1165:DHOTAF>2.3.CO;2.

Cardozo, N., Allmendinger, R.W., 2013. Spherical projections with OSXStereonet. Comput. Geosci. 51, 193–205. https://doi.org/10.1016/J.CAGEO.2012.07.021.

Charrier, R., Pinto, L., Rodríguez, M.P., 2007. Tectonostratigraphic evolution of the Andean orogen in Chile. In: Moreno, T., Gibbons, W. (Eds.), The Geology of Chile: London. The Geological Society of London, pp. 21–114.

Coloma, F., Valin, X., Oliveros, V., Vásquez, P., Creixell, C., Salazar, E., Ducea, M.N., 2017. Geochemistry of Permian to Triassic igneous rocks from northern Chile (28°-30°15'S): implications on the dynamics of the proto-Andean margin. Andean Geol. 44, 147–178. https://doi.org/10.5027/andgeoV44n2-a03.

Contreras, J.P., Espinoza, M., De la Cruz, R., Jorquera, R., Kraus, S., Ramírez, C., Naranjo, J.A., Escribano, J., Martínez, P., 2013. Carta Cifuncho, Regiones de Antofagasta y Atacama. Servicio Nacional de Geología y Minería: carta Geológica de Chile. scale 1:100,000, 1 sheet Serie Geología Básica 161, 91. p. text.

Dallmeyer, D., Brown, M., Grocott, J., Taylor, G.K., Treloar, P., 1996. Mesozoic magmatic and tectonic events within the Andean plate boundary zone, north Chile. J. Geol. 104, 19–40. https://doi.org/10.1086/629799.

del Rey, A., Deckart, K., Arriagada, C., Martínez, F., 2016. Resolving the paradigm of the late Paleozoic–Triassic Chilean magmatism: isotopic approach. Gondwana Res. 37, 172–181. https://doi.org/10.1016/j.gr.2016.06.008.

Díaz-Alvarado, J., Galaz, G., Oliveros, V., Creixell, C., Calderón, M., 2019. In: Horton, B. K., Folguera, A. (Eds.), Fragments of the Late Paleozoic Accretionary Complex in Central and Northern Chile: Similarities and Differences as a Key to Decipher the Complexity of the Late Paleozoic to Triassic Early Andean Events. Elsevier, pp. 509–530. https://doi.org/10.1016/B978-0-12-816009-1.00017-4.

Escribano, J., Martínez, P., Domagala, J., Padel, M., Espinoza, M., Jorquera, R., Contreras, J., De la Cruz, R., Calderón, M., 2013. Cartas Bahía Isla Blanca y Taltal, Región de Antofagasta. Servicio Nacional de Geología y Minería: carta Geológica de Chile. scale 1:100,000, 1 sheet Serie Geología Básica 164–165, 75. p. text.

Espinoza, M., Contreras, J.P., Jorquera, R., De La Cruz, R., Kraus, S., Ramírez, C., 2014. Carta Cerro del Pingo, Regiones de Antofagasta y Atacama: servicio Nacional de Geología y Minería, Carta Geológica de Chile. scale 1:100.000, 1 sheet Serie Geología Básica 169, 109. p. text.

Fuentes, P., Díaz-Alvarado, J., Fernández, C., Díaz-Azpiroz, M., Rodríguez, N., 2016. Structural analysis and shape-preferred orientation determination of the mélange facies in the Chañaral mélange, Las Tórtolas Formation, Coastal Cordillera, northern Chile. J. S. Am. Earth Sci. 67, 40–56. https://doi.org/10.1016/j.jsames.2016.02.001.

Fuentes, P., Díaz-Alvarado, J., Rodríguez, N., Fernández, C., Breitkreuz, C., Contreras, A. A., 2018. Geochemistry, petrogenesis and tectonic significance of the volcanic rocks of the Las Tortolas Formation, Coastal Cordillera, northern Chile. J. S. Am. Earth Sci. 87, 66–86. https://doi.org/10.1016/J.JSAMES.2017.11.006.

Fuentes, P., Fernández, C., Díaz-Alvarado, J., Díaz-Azpiroz, M., 2019. Using 3D kinematic models in subduction channels. The case of the Chañaral tectonic mélange. Coastal Cordillera, northern Chile: Gondwana Res. 74, 251–270. https://doi.org/10.1016/j.gr.2018.12.009.

Gianni, G.M., Navarrete, C.R., 2022. Catastrophic slab loss in southwestern Pangea preserved in the mantle and igneous record. Nat. Commun. 13 https://doi.org/10.1038/s41467-022-28290-z.

Godoy, E., Lara, L., 1999. Hoja Puerto Flamenco, Región de Atacama: Servicio Nacional de Geología y Minería Mapas Geológicos, vol. 15 scale 1:100,000, 1 sheet.
Godoy, E., Lara, L., 1998. Hojas chañaral y diego de Almagro, región de Atacama. Servicio Nacional de Geología y Minería Mapas Geológicos 5–6 scale 1:100,000, 1 sheet.
Godoy, E., Marquardt, C., Blanco, N., 2003. Carta Caldera, Región de Atacama: servicio Nacional de Geología y Minería, Carta Geológica de Chile. scale 1:100,000, 1 sheet Serie Geología Básica 76, 38. text.
Grocott, J., Brown, M., Dallmeyer, R.D., Taylor, G.K., Treloar, P.J., 1994. Mechanisms of Continental Growth in Extensional Arcs: an Example from the Andean Plate-Boundary Zone: Geology, vol. 22, pp. 391–394. https://doi.org/10.1130/0091-7613(1994)022<0391:MOCGIE>2.3.CO;2.
Grocott, J., Taylor, G.K., 2002. Magmatic arc fault systems, deformation partitioning and emplacement of granitic complexes in the Coastal Cordillera, north Chilean Andes (25°30′S to 27°00′S). J. Geol. Soc. 159, 425–443. https://doi.org/10.1144/0016-764901-124.
Groome, W.G., Johnson, S.E., Koons, P.O., 2006. The effects of porphyroblast growth on the effective viscosity of metapelitic rocks: implications for the strength of the middle crust. J. Metamorph. Geol. 24, 389–407. https://doi.org/10.1111/j.1525-1314.2006.00644.x.
Hervé, M., 1987. Movimiento sinistral en el Cretácico Inferior de la Zona de Falla Atacama al norte de Paposo (24°S). Rev. Geol. Chile 31, 31–42.
Jara, J.J., Barra, F., Reich, M., Leisen, M., Romero, R., Morata, D., 2021a. Episodic construction of the early Andean Cordillera unravelled by zircon petrochronology. Nat. Commun. 12, 4930. https://doi.org/10.1038/s41467-021-25232-z.
Jara, J.J., Barra, F., Reich, M., Morata, D., Leisen, M., Romero, R., 2021b. Geochronology and petrogenesis of intrusive rocks in the Coastal Cordillera of northern Chile: insights from zircon U-Pb dating and trace element geochemistry. Gondwana Res. 93, 48–72. https://doi.org/10.1016/j.gr.2021.01.007.
Kociánová, L., Melichar, R., 2016. OATools: an ArcMap add-in for the orientation analysis of geological structures. Comput. Geosci. 87, 67–75. https://doi.org/10.1016/j.cageo.2015.12.005.
Kylander-Clark, A.R.C., Hacker, B.R., Cottle, J.M., 2013. Laser-ablation split-stream ICP petrochronology. Chem. Geol. 345, 99–112. https://doi.org/10.1016/j.chemgeo.2013.02.019.
Lara, L., Godoy, E., 1998. Hoja Quebrada salitrosa, región de Atacama: servicio nacional de Geología y minería. Mapas Geológicos 4 scale 1:100,000, 1 sheet.
Law, R.D., 2014. Deformation thermometry based on quartz c-axis fabrics and recrystallization microstructures: a review. J. Struct. Geol. 66, 129–161. https://doi.org/10.1016/J.JSG.2014.05.023.
Masoch, S., Gomila, R., Fondriest, M., Jensen, E., Mitchell, T., Pennacchioni, G., Cembrano, J., di Toro, G., 2021. Structural evolution of a crustal-scale seismogenic fault in a magmatic arc: the Bolfin fault zone (Atacama fault system). Tectonics 40. https://doi.org/10.1029/2021TC006818 e2021TC006818.
Matthews, K.J., Maloney, K.T., Zahirovic, S., Williams, S.E., Seton, M., Müller, R.D., 2016. Global plate boundary evolution and kinematics since the late Paleozoic. Global Planet. Change 146, 226–250. https://doi.org/10.1016/J.GLOPLACHA.2016.10.002.
Mavor, S.P., Singleton, J.S., Gomila, R., Heuser, G., Seymour, N.M., Williams, S.A., Arancibia, G., Johnston, S.M., Kylander-Clark, A.R.C., Stockli, D.F., 2020. Timing, kinematics, and displacement of the Taltal fault system, northern Chile: implications for the cretaceous tectonic evolution of the andean margin. Tectonics 39. https://doi.org/10.1029/2019TC005832 e2019TC005832.
Oliveros, V., Vásquez, P., Creixell, C., Lucassen, F., Ducea, M.N., Ciocca, I., González, J., Espinoza, M., Salazar, E., Coloma, F., Kasemann, S.A., 2020. Lithospheric evolution of the pre- and early andean convergent margin, Chile. Gondwana Res. 80, 202–227. https://doi.org/10.1016/j.gr.2019.11.002.
Passchier, C.W., Trouw, R.A.J., 2005. Microtectonics. Springer, Berlin, p. 366.
Paterson, S.R., Vernon, R.H., Tobisch, O.T., 1989. A review of criteria for the identification of magmatic and tectonic foliations in granitoids. J. Struct. Geol. 11, 349–363. https://doi.org/10.1016/0191-8141(89)90074-6.
Pattison, D.R.M., Spear, F.S., 2018. Kinetic control of staurolite–Al_2SiO_5 mineral assemblages: implications for Barrovian and Buchan metamorphism. J. Metamorph. Geol. 36, 667–690. https://doi.org/10.1111/jmg.12302.
Prinz, P., Wilke, H.-G., von Hillebrandt, A., 1994. Sediment accumulation and subsidence history in the Mesozoic marginal basin of northern Chile. In: Reutter, K.-J., Scheuber, E., Wigger, P.J. (Eds.), Tectonics of the Southern Central Andes. Springer-Verlag, Berlin, Heidelberg, pp. 219–232. https://doi.org/10.1007/978-3-642-77353-2_15.
Ring, U., Willner, A.P., Layer, P.W., Richter, P.P., 2012. Jurassic to Early Cretaceous postaccretional sinistral transpression in north-central Chile (latitudes 31-32°S). Geol. Mag. 149, 208–220. https://doi.org/10.1017/S0016756811000653.
Rodríguez, N., Díaz-Alvarado, J., Fernández, C., Breitkreuz, C., Fuentes, P., Merida, G., 2021. Relation between intrusive and deformational processes in oblique subductive margins. The case of the zoned Flamenco pluton in northern Chile. J. S. Am. Earth Sci. 112, 103553 https://doi.org/10.1016/J.JSAMES.2021.103553.
Rodríguez, N., Díaz-Alvarado, J., Fernández, C., Fuentes, P., Breitkreuz, C., Tassinari, C. C.G., 2019. The significance of U-Pb zircon ages in zoned plutons: the case of the Flamenco pluton, Coastal Range batholith, northern Chile. Geosci. Front. 10, 1073–1099. https://doi.org/10.1016/j.gsf.2018.06.003.
Ruthven, R., Singleton, J., Seymour, N., Gomila, R., Arancibia, G., Stockli, D.F., Ridley, J., Magloughlin, J., 2020. The geometry, kinematics, and timing of deformation along the southern segment of the Paposo fault zone, Atacama fault system, northern Chile. J. S. Am. Earth Sci. 97, 102355 https://doi.org/10.1016/J.JSAMES.2019.102355.
Saldías, J., Espinoza, M., Astudillo, N., Contreras, J., Arriagada, C., 2015. Origen de la fábrica magnética de la Granodiorita Cerro del Pingo, norte de Chile (25°40′S – 70°15′O): implicancias en relación a su mecanismo de emplazamiento. Congreso Geológico Chileno 14, 530–533. La Serena, Chile.
Sanderson, D.J., Marchini, W.R.D., 1984. Transpression. J. Struct. Geol. 6, 449–458. https://doi.org/10.1016/0191-8141(84)90058-0.
Scheuber, E., Andriessen, P.A.M., 1990. The kinematic and geodynamic significance of the Atacama fault zone, northern Chile. J. Struct. Geol. 12, 243–257. https://doi.org/10.1016/0191-8141(90)90008-M.
Scheuber, E., Bogdanic, T., Jensen, A., Reutter, K.-J., 1994. Tectonic development of the north Chilean Andes in relation to plate convergence and magmatism since the jurassic. In: Reutter, K.-J., Scheuber, E., Wigger, P.J. (Eds.), Tectonics of the Southern Central Andes. Springer Berlin Heidelberg, Berlin, Heidelberg, pp. 121–139. https://doi.org/10.1007/978-3-642-77353-2_9.
Scheuber, E., Gonzalez, G., 1999. Tectonics of the Jurassic-Early Cretaceous magmatic arc of the north Chilean Coastal Cordillera (22°-26°S): a story of crustal deformation along a convergent plate boundary. Tectonics 18, 895–910. https://doi.org/10.1029/1999TC900024.
Scheuber, E., Hammerschmidt, K., Friedrichsen, H., 1995. $^{40}Ar/^{39}Ar$ and Rb-Sr analyses from ductile shear zones from the Atacama Fault Zone, northern Chile: the age of deformation. Tectonophysics 250, 61–87. https://doi.org/10.1016/0040-1951(95)00044-8.
Scheuber, E., Reutter, K.-J., 1992. magmatic arc tectonics in the central Andes between 21° and 25°S. Tectonophysics 205, 127–140. https://doi.org/10.1016/0040-1951(92)90422-3.
Seton, M., et al., 2012. Global continental and ocean basin reconstructions since 200 Ma. Earth Sci. Rev. 113, 212–270. https://doi.org/10.1016/J.EARSCIREV.2012.03.002.
Seymour, N.M., Singleton, J.S., Gomila, R., Mavor, S.P., Heuser, G., Arancibia, G., Williams, S., Stockli, D.F., 2021. Magnitude, timing, and rate of slip along the Atacama fault system, northern Chile: implications for Early Cretaceous slip partitioning and plate convergence. J. Geol. Soc. 178, jgs2020–j2142. https://doi.org/10.1144/jgs2020-142.
Seymour, N.M., Singleton, J.S., Mavor, S.P., Gomila, R., Stockli, D.F., Heuser, G., Arancibia, G., 2020. The relationship between magmatism and deformation along the intra-arc strike-slip Atacama fault system, northern Chile. Tectonics 39. https://doi.org/10.1029/2019TC005702 e2019TC005702.
Stenvall, C.A., Fagereng, Å., Diener, J.F.A., 2019. Weaker than weakest: on the strength of shear zones. Geophys. Res. Lett. 46, 7404–7413. https://doi.org/10.1029/2019GL083388.
Stipp, M., Stünitz, H., Heilbronner, R., Schmid, S.M., 2002. Dynamic Recrystallization of Quartz: Correlation between Natural and Experimental Conditions, vol. 200. Geological Society Special Publication. https://doi.org/10.1144/GSL.SP.2001.200.01.11.
Stipp, M., Tullis, J., 2003. The recrystallized grain size piezometer for quartz. Geophys. Res. Lett. 30 https://doi.org/10.1029/2003GL018444.
Taylor, G.K., Randall, D.E., 2000. Structural analysis of dyke emplacement directions as an aid to palaeomagnetic studies: an example from northern Chile. Geophys. J. Int. 141, 252–258. https://doi.org/10.1046/j.1365-246x.2000.00064.x.
Tetley, M.G., Williams, S.E., Gurnis, M., Flament, N., Müller, R.D., 2019. Constraining absolute plate motions since the triassic. J. Geophys. Res. Solid Earth 124, 7231–7258. https://doi.org/10.1029/2019JB017442.
Vermeesch, P., 2018. IsoplotR: a free and open toolbox for geochronology. Geosci. Front. 9, 1479–1493. https://doi.org/10.1016/J.GSF.2018.04.001.
Vollmer, F.W., 1990. An application of eigenvalue methods to structural domain analysis. GSA Bulletin 102, 786–791. https://doi.org/10.1130/0016-7606(1990)102<0786:AAOEMT>2.3.CO;2.
Young, A., Flament, N., Maloney, K., Williams, S., Matthews, K., Zahirovic, S., Müller, R. D., 2019. Global kinematics of tectonic plates and subduction zones since the late Paleozoic Era. Geosci. Front. 10, 989–1013. https://doi.org/10.1016/J.GSF.2018.05.011.